Submitted to Earthquake Engineering and Structural Dynamics

Received: Added at production | Revised: Added at production | Accepted: Added at production

DOI: xxx/xxxx

RESEARCH ARTICLE

Sequential sampling approach to energy-based multi-objective design optimization of steel frames with correlated random parameters

Bach Do* | Makoto Ohsaki

Department of Architecture and Architectural Engineering, Graduate School of Engineering, Kyoto University, Kyoto, Japan

Correspondence
*Bach Do, Department of Architecture and Architectural Engineering, Graduate School of Engineering, Kyoto University, Kyoto-Daigaku Katsura, Nishikyo, Kyoto 615-8540, Japan. Email: se.do@archi.kyoto-u.ac.jp

Abstract

This work presents a novel sequential sampling approach to the multi-objective reliability-based design optimization of moment-resisting steel frames subjected to earthquake excitation. The optimization problem is formulated with two objective functions, namely, the total mass and the energy dissipated by beam members of the frame, and subject to uncorrelated probabilistic constraints on dynamic responses under the effects of correlated random parameters of floor masses, external loads, and material properties. The dynamic responses for a small number of designs are found by nonlinear response history analysis and further approximated by Gaussian process (GP) models to mitigate the computational burden during the optimization process. Approximate solutions sorted among existing candidate solutions are updated after each optimization iteration using discrete random local and global searches. The GP models are also refined after each optimization iteration by specifying new sampling points that lie on the Pareto front of a bi-objective deterministic maximization problem formulated for the improvement in the current approximate solutions and the feasibility of the new sampling points. As demonstrated in a test problem, the new sampling points tend to distribute in the neighborhood of the exact solutions, thereby underpinning a quick termination as well as the robustness of the proposed method. Optimization results from the test problem and a design example show that good approximate solutions are always obtained as the solution quality converges.

KEYWORDS:
sequential optimization, energy dissipation, probabilistic constraints, correlated random parameters, multi-objective optimization, steel frames

1 | INTRODUCTION

Inherent uncertainty in external loads and material properties has important effects on structural performance.[1,2] Addressing these effects to ensure structural safety is one of the main subjects of structural design codes.[3,4] Each design code uses deterministic safety measures of partial load and resistance factors for simultaneously amplifying the effects of uncertain external loads on structural behavior and reducing the resistance capacity of structural members subjected to uncertain material properties. The goal is to produce a conservative design that is associated with a safety margin of the reduced resistance capacity and the sum of amplified load effects. This design approach is particularly appealing because it allows practicing engineers to adopt

a simple way for addressing the two ingredients of a safety measure simultaneously. However, it may suffer from lack of invariability as different sets of partial factors can be found for a particular limit state.[5] The design approach may also not address the cost issues of a structure properly as it only manages the trade-off between safety and cost aspects in a general context for similar structures[6] rather than a rigorous reliability calculation for a particular structure. Thus, it is desirable to use a unified approach integrating probabilistic safety measures and optimization algorithms for handling both the safety and cost issues of structures.

The literature provides three different methods for such a unified approach, namely, robust design optimization (RDO),[7–12] reliability-based design optimization (RBDO),[13–16] and risk-based optimization (RBO).[17] These methods differs in how unfavorable effects of uncertainty can be managed. The RDO commonly evaluates the sensitivity of uncertain structural responses and uses this information for finding a design that is less sensitive at an acceptable cost. The RBDO seeks a minimum-cost design that, under uncertainty, guarantees an allowable probability of occurring structural failures while ignoring the expected cost due to these failures. Meanwhile, the RBO minimizes a total cost of structural and expected-failure costs. Although their formulations are different, the three methods encounter the same difficulty in finding a good compromise between processing optimization and propagating uncertainty. By focusing on solving a bi-objective RBDO problem of elastic-plastic moment-resisting steel frames subjected to earthquake excitation, this study presents an efficient approach to resolving the aforementioned issue.

The RBDO problem is formulated with two objective functions, namely, the total mass and energy dissipated by beam members of the frame. The goal is to find a minimum-cost design for maximum energy dissipation of the beams during earthquake excitation.[18] The problem is subject to uncorrelated probabilistic constraints on dynamic responses of the frame under the effects of correlated random parameters of floor masses, external loads, and material properties. The dynamic responses of interest are evaluated using nonlinear response history analysis (NRHA),[19,20] thereby enabling an accurate simulation of the plastic mechanism of the structure. To the authors' knowledge, this is the first time the NRHA is used for seismic design considering uncertainty as previous studies for such a design have only adopted nonlinear static pushover analysis.[21–23] The NRHA, however, increases the complexity of the RBDO problem. Thus, it a pressing need for devising a new optimization strategy that keeps the advantages of the NRHA while reducing the computational cost due to incorporating uncertainty propagation into optimization.

Solving the bi-objective RBDO problem encounters the following five difficulties. First, the dynamic responses for evaluating the uncertain energy dissipation of the beams and the probabilistic constraints are highly nonlinear and implicit within the NRHA program. Therefore, it is computationally intractable to guide the optimization process by direct evaluations of these responses. Second, it is very difficult to find exact solutions to the RBDO problem considered in this study because its feasible space defined by the probability function is intrinsically nonconvex. Existing approaches, such as scenario and convex approximation approaches, can solve the problem approximately with special forms of the probabilistic constraint functions.[24] Third, calculating the failure probabilities of the probabilistic constraints suffers from inherent drawbacks of conventional reliability analysis methods, for example, poor performance of the first- and second-order reliability methods[25] when handling highly nonlinear limit state functions (LSFs) or the curse of dimensionality when using the Monte-Carlo simulation (MCS) for high-dimensional problems. Fourth, it is computationally expensive to evaluate the expected value of the uncertain energy dissipation of the beams. Although the MCS, polynomial chaos expansion,[26] and Monte-Carlo integration[27] can carry out this task, they are all subject to the curse of dimensionality that requires many calls of the NRHA for a reliable expected value. The Bayes-Hermite quadrature[28] and Taylor series approximation[29] can also be used with respective restrictions that the random parameters are independent and normally distributed and the energy dissipation function should be differentiable with respect to the random parameters. Finally, even though adaptive approaches using surrogate models have solved complex RBDO problems effectively,[30] the discrete and multi-objective nature of the RBDO problem in this study may hinder the application of these approaches.

To address the above difficulties, this work proposes a sequential sampling approach whose main features are as follows:

1. The dynamic responses for a small number of designs are evaluated using the NRHA. The corresponding uncertain LSFs are then approximated by Gaussian process (GP) models for carrying out the optimization process. These GP models make easy use of the MCS for evaluating expected value of the uncertain dissipation energy of the beams as well as the probabilistic constraints of the RBDO problem.

2. Approximate solutions to the bi-objective RBDO problem sorted from existing candidate solutions are strategically updated after each optimization iteration. The updated candidate solutions consist of the available candidates and new candidates generated by performing discrete random local and global searches.

3. The GP models for the uncertain LSFs are refined after each optimization iteration by specifying a batch of new sampling points that lie on the Pareto front of a bi-objective deterministic maximization problem formulated for addressing the

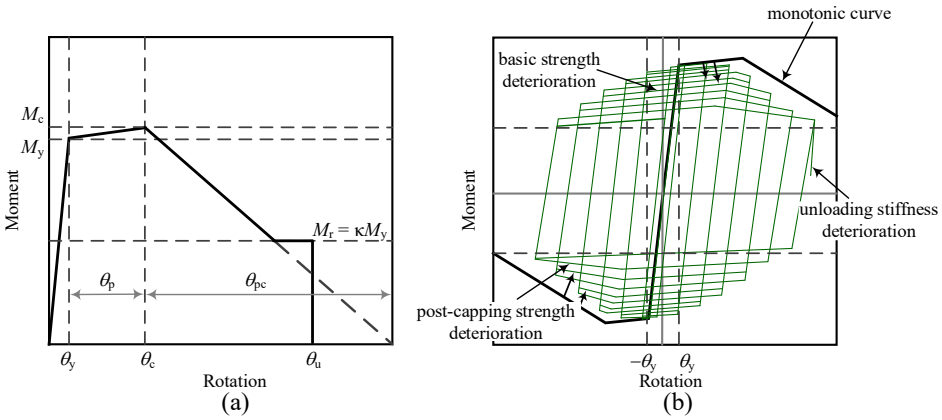

FIGURE 1 Modified IK deterioration model for semi-rigid rotational springs: (a) monotonic curve; (b) basic modes for cyclic deterioration (Adapted from Ref.[31]).

improvement in the current solutions and the feasibility of the new sampling points simultaneously. This refinement scheme differs from those of other sequential optimization methods, such as Bayesian optimization[12] or a sequential method by the authors,[16] where only one new sampling point is specified after each optimization iteration. As will be demonstrated in a test problem, the new sampling points tend to distribute in the neighborhood of exact solutions, leading to the robustness of the refinement scheme as well as a quick termination of the optimization process.

The remainder of this paper progresses as follows. Section 2 formulates the bi-objective RBDO problem, followed by the selection of recorded ground motions in Section 3. Section 4 details the proposed optimization method. Its performance is carefully verified against a simple bi-objective RBDO problem of a two-bar truss in Section 5. Section 6 uses the proposed method for solving the RBDO problem of a planar moment-resisting steel frame. Finally, Section 7 concludes this paper. Appendix provides the mathematical foundation of the GP model.

2 | ENERGY-BASED DESIGN OPTIMIZATION PROBLEM OF MOMENT-RESISTING STEEL FRAMES

Consider a moment-resisting steel frame subjected to vertical and earthquake loads. The frame is designed according to the capacity-design principle, by which the structural components are classified into dissipative and non-dissipative members. The dissipative members, through their inelastic deformations, are primarily responsible for dissipating seismic energy. The failure of these members must occur prior to that of the non-dissipative members to prevent brittle collapse of the whole structure. As beam members of the frame serve as the dissipative members,[20] they are expected to experience large inelastic deformations during the earthquake.

This section first describes the evaluation of energy dissipated by the beams using their internal force-deformation histories from the NRHA. It then formulates the bi-objective RBDO problem for the frame based on the evaluated energy.

2.1 | Dissipation energy of beam members

The energy balance equation of the multi-degree-of-freedom system for the frame during the earthquake excitation gives[32]

$$E_k^t + E_d^t + E_p^t = E_i^t \tag{1}$$

where E_k^t, E_d^t, E_p^t, and E_i^t represent the kinetic, damping, dissipation, and input energies at a time instant t, respectively.

E_p^t including recoverable-elastic strain and irrecoverable-plastic energies of all structural members can be evaluated based on the force-deformation histories of these members. When the elastoplastic behavior of each member is simulated using an elastic beam-column element in the middle and two semi-rigid rotational springs with hysteretic properties at the member ends,[33] E_p^t can be directly derived from moment-rotation histories of these springs.

The cyclic behavior of the rotational springs may follow a bilinear hysteretic response incorporated in the modified Ibarra Krawinkler (IK) deterioration model, as depicted in Figure 1.[31] This model provides strength bounds for the spring using a monotonic curve and a cyclic damage rule that captures the deterioration of the bounds as the cyclic excursion accumulates. The monotonic curve is characterized by three strength parameters and four deformation parameters. Three strength parameters include (1) the effective yield moment M_y, equal to 1.1 times the plastic moment of the section obtained from plastic section modulus and the material yield strength σ_y;[31] (2) the capping moment strength M_c, described by a post-yield strength ratio M_c/M_y; and (3) the residual moment M_r, defined by a residual strength ratio κ, i.e., $M_r = \kappa M_y$. Four deformation parameters consist of (1) the yield rotation θ_y; (2) the pre-capping plastic rotation for monotonic loading θ_p; (3) the post-capping plastic rotation θ_{pc}; and (4) the ultimate rotation capacity θ_u, assigned as 0.06 rad.[23,31]

Let $E_r = \lambda M_y$ denote a reference hysteretic energy dissipation capacity of each spring, where λ is the so-called reference cumulative rotation capacity. The rate of cyclic deterioration of the spring in the current excursion can be expressed as a function of E_r, the hysteretic energy dissipated in the current excursion, and the total energy dissipated in past excursions. Detailed expression for such a cyclic deterioration rate can be found in the seminal work by Lignos and Krawinkler.[31]

As the energy dissipated by the mentioned beam-column element is primarily due to flexure, the dissipation energy of the ith beam and that of the ith column at time t, denoted as $E^t_{pb,i}$ and $E^t_{pc,i}$, can be evaluated using the following discrete expressions.

$$E^t_{pb,i} = E^{t-\Delta t}_{pb,i} + \frac{M^t_{b1,i} + M^{t-\Delta t}_{b1,i}}{2}\Delta\theta_{b1,i} + \frac{M^t_{b2,i} + M^{t-\Delta t}_{b2,i}}{2}\Delta\theta_{b2,i} \tag{2}$$

$$E^t_{pc,i} = E^{t-\Delta t}_{pc,i} + \frac{M^t_{c1,i} + M^{t-\Delta t}_{c1,i}}{2}\Delta\theta_{c1,i} + \frac{M^t_{c2,i} + M^{t-\Delta t}_{c2,i}}{2}\Delta\theta_{c2,i} \tag{3}$$

where $t - \Delta t$ and t denote two consecutive time instants; $M_{b(c)1}$ and $M_{b(c)2}$ stand for internal moments of the first (1) and second (2) semi-rigid rotational springs of the beam (column) element, respectively; and $\Delta\theta_{b(c)1(2),i} = \theta^t_{b(c)1(2),i} - \theta^{t-\Delta t}_{b(c)1(2),i}$ with $\theta_{b(c)1}$ and $\theta_{b(c)2}$ represent rotation angles of the first (1) and second (2) rotational springs of the beam (column) element, respectively.

Let E_{pb} and E_{pc} represent the energies dissipated by n_b beams and n_c columns of the frame at the end of the earthquake, respectively. The dissipation energy ratio of the beams reads

$$\beta = E_{pb}/\left(E_{pb} + E_{pc}\right) = \sum_{i=1}^{n_b} E_{pb,i} \Big/ \left(\sum_{i=1}^{n_b} E_{pb,i} + \sum_{j=1}^{n_c} E_{pc,j}\right) \tag{4}$$

2.2 | Formulation of the RBDO problem

Let $\mathbf{s} = [s_1, ..., s_{d_1}]^T \subset \mathbb{N}^{d_1}$ be a d_1-dimensional vector of discrete design variables of the frame, and $\mathbf{r} = [r_1, ..., r_{d_2}]^T \subset \mathbb{R}^{d_2}$ be a d_2-dimensional vector of continuous random parameters of floor masses, vertical loads, and material properties. Each element of $\mathbf{s}$ corresponds to a section number in a list of American wide-flange steel sections, i.e., $s_k \in S_k\,(k = 1, \ldots, d_1)$, while probabilistic characteristics of $\mathbf{r}$ are described by the marginal probability density functions (PDFs), or equivalently, the cumulative distribution functions (CDFs) of its elements. The elements of $\mathbf{r}$ correlate with each other according to a given correlation matrix.

The RBDO problem is formulated for the frame to optimize the steel section of its members considering its total mass and the dissipation energy of the beams. The first objective function associated with the total mass of the frame reads

$$f_1(\mathbf{s}) = \sum_{i=1}^{n_e} \rho_i L_i / m_{max} \tag{5}$$

where L_i, ρ_i, and n_e denote the length of the ith member, nominal mass [kg/m] of the steel section of the ith member, and the number of members, respectively; and m_{max} is the maximum value of the total mass. Possible values of $f_1(\mathbf{s})$ range from 0 to 1.

The second objective function corresponds to the expected dissipation energy ratio of all beam members as given in Equation (4). For a minimization problem, this objective function is formulated with the minus sign as

$$f_2(\mathbf{s}) = -\mathbb{E}[\beta(\mathbf{s}, \mathbf{r})] \tag{6}$$

where $\mathbb{E}[\cdot]$ represents the mean of $[\cdot]$ with respect to $\mathbf{r}$. As $0 < \beta(\mathbf{s}, \mathbf{r}) < 1$, $f_2(\mathbf{s})$ ranges from -1 to 0. When using a total of n_g ground motions for the design, which are assumed to have the same duration, $\beta(\mathbf{s}, \mathbf{r})$ is defined as the mean value of the dissipation energy ratios for these motions.

To ensure the frame remains intact during the earthquake, the maximum inter-story drift and maximum plastic rotation of the member ends are limited by some thresholds. Conventionally, plastic deformations are not allowed for the columns. This study, however, allows the columns to have minor plastifications because minimizing their dissipation energy is consistent with maximizing the dissipation energy of the beams. Let $\delta(\mathbf{s},\mathbf{r})$, $\varphi(\mathbf{s},\mathbf{r})$, and $\omega(\mathbf{s},\mathbf{r})$ denote uncertain LSFs corresponding to the absolute maximum of the inter-story drift ratios, absolute maximum of the beam-end plastic rotations, and absolute maximum of the column-end plastic rotations during the earthquake, respectively; and δ_a, φ_a, and ω_a be the respective allowable thresholds. Accordingly, the LSFs corresponding to the inter-story drift and member-end plastic rotations read

$$\delta(\mathbf{s},\mathbf{r}) = \max\left(|\delta_1|,\ldots,|\delta_{n_\mathrm{s}}|\right)/\delta_\mathrm{a} - 1 \tag{7}$$
$$\varphi(\mathbf{s},\mathbf{r}) = \max\left(|\varphi_1|,\ldots,|\varphi_{2n_\mathrm{b}}|\right)/\varphi_\mathrm{a} - 1 \tag{8}$$
$$\omega(\mathbf{s},\mathbf{r}) = \max\left(|\omega_1|,\ldots,|\omega_{2n_\mathrm{c}}|\right)/\omega_\mathrm{a} - 1 \tag{9}$$

where δ_i is the inter-story drift ratio of the ith story, defined as the ratio of the story drift to the corresponding story height; and n_s represents the number of stories. The inter-story drift ratio, beam-end rotation, and column-end rotation at a particular time instant are evaluated as the mean value of the corresponding responses for n_g ground motions.

To ensure a column or a beam member can sustain the plastic moment without exhibiting local buckling, the width-thickness ratio of all plates composing the steel section of that member should be constrained. In accordance with Chapter B of AISC 360-16,[3] the following two constraints are applied to the web and flange plates of the section of each member, respectively.

$$g_1(\mathbf{s}) = \frac{d-2t_\mathrm{f}}{t_\mathrm{w}} - 3.76\sqrt{\frac{\mathbb{E}[E]}{\mathbb{E}[\sigma_\mathrm{y}]}} \le 0 \tag{10}$$

$$g_2(\mathbf{s}) = \frac{b}{2t_\mathrm{f}} - 0.38\sqrt{\frac{\mathbb{E}[E]}{\mathbb{E}[\sigma_\mathrm{y}]}} \le 0 \tag{11}$$

where d, b, t_f, and t_w are the height, flange width, flange thickness, and web thickness, respectively; and E and σ_y are Young's modulus and initial yield stress of the steel material, respectively.

Furthermore, a total of J constructional constraints $l_j(\mathbf{s}) \le 0$, $j = 1,\ldots,J$, are imposed at beam-column connections and column-column joints. The goal is to ensure (1) the flange width of a beam connected to a column is less than or equal to the flange width of the column and (2) the depth of the column section in the upper story should not exceed that in the lower story.

Using the above objective and constraint functions, the bi-objective RBDO problem formulated for the frame to optimize its total mass and the dissipation energy of its beams can be stated as follows:

$$\begin{aligned}
\min_{\mathbf{s}}. \quad & \left[f_1(\mathbf{s}), f_2(\mathbf{s})\right] \\
\text{subject to} \quad & \mathbb{P}\left[\delta(\mathbf{s},\mathbf{r}) \le 0\right] \ge 1-\epsilon_1 \\
& \mathbb{P}\left[\varphi(\mathbf{s},\mathbf{r}) \le 0\right] \ge 1-\epsilon_2 \\
& \mathbb{P}\left[\omega(\mathbf{s},\mathbf{r}) \le 0\right] \ge 1-\epsilon_3 \\
& g_i(\mathbf{s}) \le 0,\ i = 1,..2d_1 \\
& l_j(\mathbf{s}) \le 0,\ j = 1,..J \\
& s_i \in S_i,\ i = 1,..d_1
\end{aligned} \tag{12}$$

where $\mathbb{P}[\cdot]$ denotes the probability of occurring $[\cdot]$ with respect to $\mathbf{r}$; and ϵ_1, ϵ_2, and ϵ_3 are acceptable risk levels, supported on $(0, 1)$ and specified by the designer. As a connection to current design codes, these risk levels can be derived from corresponding target reliability values specified in each design code. The problem is limited to element reliability as the frame is not functional if one of the individual probabilistic constraints is violated.

Moving the left-side terms of the probabilistic constraints in problem (12) to the right side and let

$$\delta(\mathbf{s}) = 1 - \epsilon_1 - \mathbb{P}\left[\delta(\mathbf{s},\mathbf{r}) \le 0)\right] \tag{13}$$
$$\varphi(\mathbf{s}) = 1 - \epsilon_2 - \mathbb{P}\left[\varphi(\mathbf{s},\mathbf{r}) \le 0)\right] \tag{14}$$
$$\omega(\mathbf{s}) = 1 - \epsilon_3 - \mathbb{P}\left[\omega(\mathbf{s},\mathbf{r}) \le 0)\right] \tag{15}$$

Thus, problem (12) can be rewritten as

$$\begin{aligned} \min_{\mathbf{s}}. \quad & \left[f_1(\mathbf{s}), f_2(\mathbf{s})\right] \\ \text{subject to} \quad & \delta(\mathbf{s}) \le 0, \ \ \varphi(\mathbf{s}) \le 0, \ \ \omega(\mathbf{s}) \le 0 \\ & g_i(\mathbf{s}) \le 0, \ i = 1, ..2d_1 \\ & l_j(\mathbf{s}) \le 0, \ j = 1, ..J \\ & s_i \in S_i, \ i = 1, ..d_1 \end{aligned} \tag{16}$$

Exact Pareto-optimal solutions to problem (16) are difficult to obtain because $f_2(\mathbf{s})$, $\delta(\mathbf{s})$, $\varphi(\mathbf{s})$, and $\omega(\mathbf{s})$ are nonlinear, non-convex, and implicit within the NRHA program. A new optimization strategy, therefore, is proposed for solving the problem approximately.

3 | DESIGN RESPONSE SPECTRUM AND SCALING RECORDED GROUND MOTIONS

According to ASCE 7-16,[4] the design spectral response acceleration S_a can be evaluated using the risk-targeted maximum considered earthquake (MCE_R). The MCE_R is constructed based on the uniform-hazard (2% in 50-year) ground motions, which underline the ASCE 7-16 MCE_R ground motion maps. Let S_S and S_1 denote the mapped MCE_R, 5%-damped, spectral response acceleration parameters at short periods and at a period of 1 s, respectively. Design values of S_S and S_1, denoted as S_{DS} and S_{D1}, are determined as[4]

$$S_{DS} = \frac{2}{3} F_a S_S, \quad S_{D1} = \frac{2}{3} F_v S_1 \tag{17}$$

where F_a and F_v are two coefficients considering the site soil properties.

Once S_{DS} and S_{D1} are obtained, S_a reads[4]

$$S_a = \begin{cases} S_{DS}\left(0.4 + 0.6T/T_0\right) & \text{if } T \le T_0 \\ S_{DS} & \text{if } T_0 < T \le T_s \\ S_{D1}/T & \text{if } T_s < T \le T_L \\ S_{D1}T_L/T^2 & \text{if } T > T_L \end{cases} \tag{18}$$

where T denotes the fundamental natural period of the structure; $T_0 = 0.2S_{D1}/S_{DS}$; $T_s = S_{D1}/S_{DS}$; and T_L is the long-period transition period.[4]

When different recorded earthquake ground motions are used for the design, they should be scaled such that the mean of 5%-damped response spectra for the scaled motions is not less than the design MCE_R spectrum over the period range of $0.2T - 1.5T$.[4] For the frame design in this study, a total of six recorded earthquake ground motions are selected from the Pacific Earthquake Engineering Research Center (PEERC) database,[34] as listed in Table 1. The acceleration spectra of the selected ground motions are scaled to simulate the target MCE_R acceleration spectrum using a scaling procedure by Reyes and Kalkan.[35] The design acceleration time histories of the selected motions are then evaluated by multiplying the recorded acceleration time histories by the corresponding scale factors.

4 | SOLUTION APPROACH

4.1 | Generating correlated random parameters

The vector of random parameters $\mathbf{r} = [r_1, ..., r_{d_2}]^T$ is described by the marginal PDFs or CDFs of its elements, i.e., $p_{r_i}(r_i)$ or $F_{r_i}(r_i)$, respectively. The correlations between these elements are characterized by the correlation matrix $\mathbf{\Sigma}_r$. The goal is to generate a finite number of $\mathbf{r}$ samples for processing the optimization.

Let $\mathbf{c} = [c_1, ..., c_{d_2}]^T \sim \mathcal{N}(\mathbf{0}, \mathbf{\Sigma}_r)$ denote a d_2-variate Gaussian vector in a standardized space, respectively. Samples of $\mathbf{c}$ can be generated using the built-in MATLAB function *normrnd*.[36] It is also trivial to evaluate the CDF for each sample c_i, denoted as $F_{c_i}(c_i)$, because c_i follows a standard Gaussian, i.e., $c_i \sim \mathcal{N}(0, 1)$.

Suppose there exists an iso-probabilistic mapping that transforms the physical space of $\mathbf{r}$ into the standardized space of $\mathbf{c}$. This mapping preserves the CDFs at two corresponding points r_i and c_i, i.e., $F_{r_i}(r_i) = F_{c_i}(c_i)$. Thus, the random samples of r_i

TABLE 1 Six selected ground motions.[34]

ID	Event	Year	Station	Magnitude	Fault normal component		
					PGA [g]	PGV [cm/s]	PGD [cm]
1	Imperial Valley-06	1979	Delta	6.53	0.6	63.6	30.8
2	Loma Prieta	1989	Gilroy Array ≠ 4	6.93	1.0	100.8	32.5
3	Northridge-01	1994	Canoga Park	6.69	0.8	132.2	56.7
4	Kobe Japan	1995	Kakogawa	6.90	0.5	39.2	12.8
5	Kobe Japan	1995	Shin-Osaka	6.90	0.6	89.9	26.3
6	Chi-Chi Taiwan	1991	CHY036	7.62	0.9	101.0	47.8

PGA = peak ground acceleration, PGV = peak ground velocity, PGD = peak ground displacement

can be generated by

$$r_i = F_{r_i}^{-1}\left(F_{c_i}(c_i)\right) \tag{19}$$

where $F_{r_i}^{-1}(\cdot)$ denotes the inverse CDF function with respect to r_i. It is worth noting that Equation (19) is applicable to any distributions of $\mathbf{r}$ and can also be used for generating samples of uncorrelated random parameters.

4.2 | Proposed sequential optimization approach

4.2.1 | Approximate uncertain objective and probabilistic constraint functions

As the first step of solving problem (16), $\beta(\mathbf{s},\mathbf{r})$, $\delta(\mathbf{s},\mathbf{r})$, $\varphi(\mathbf{s},\mathbf{r})$, and $\omega(\mathbf{s},\mathbf{r})$ are approximated by the corresponding GP models trained based upon a finite number of sampling points. To do so, a training dataset $\mathcal{D} = \{\mathbf{X},\mathbf{y}\} = \{\mathbf{x}_i, y_i\}_{i=1}^{N}$ is generated, where $\mathbf{x}_i = [\mathbf{s}_i^T, \mathbf{r}_i^T]^T \in \mathbb{R}^d$ ($d = d_1 + d_2$) are d-dimensional vectors of uncertain input variables, and $y_i \in \mathbb{R}$ are the corresponding outputs (β_i, δ_i, φ_i, or ω_i). The number of initial training samples N depends on the number of input variables d, for example, $N \geq 15d$.[12] Samples of $\mathbf{s}$ and $\mathbf{r}$ are generated using Latin-hypercube sampling (LHS) and Equation (19), respectively. Integer samples of $\mathbf{s}$ are determined by rounding the corresponding real samples by LHS to the nearest integers. Each sample $\mathbf{x}_i$ then serves as an input to the NRHA for evaluating the corresponding dynamic responses of interest. The samples that provide non-positive values of the LSFs $\delta(\mathbf{s},\mathbf{r})$, $\varphi(\mathbf{s},\mathbf{r})$, and $\omega(\mathbf{s},\mathbf{r})$ are retained in $\mathcal{D}$ as N feasible training samples, which are used for constructing the GP models.

A GP model establishes the relationship between the uncertain input variables $\mathbf{x} = [\mathbf{s}^T, \mathbf{r}^T]^T$ and the corresponding uncertain output y using the mapping $y = \hat{g}(\mathbf{x}) : \mathbb{R}^d \rightarrow \mathbb{R}$, where $\hat{g}(\mathbf{x})$ is a Gaussian conditioned on $\mathcal{D}$. Therefore, the GP models for $\beta(\mathbf{s},\mathbf{r})$, $\delta(\mathbf{s},\mathbf{r})$, $\varphi(\mathbf{s},\mathbf{r})$, and $\omega(\mathbf{s},\mathbf{r})$ at each realization of the input variable vector are the Gaussians $\hat{\beta}(\mathbf{s},\mathbf{r})$, $\hat{\delta}(\mathbf{s},\mathbf{r})$, $\hat{\varphi}(\mathbf{s},\mathbf{r})$, and $\hat{\omega}(\mathbf{s},\mathbf{r})$, respectively. The mean and variance characterizing each of these GP models, for example, $\mu_{\hat{\delta}(\mathbf{s},\mathbf{r})}$ and $\sigma^2_{\hat{\delta}(\mathbf{s},\mathbf{r})}$ of $\hat{\delta}(\mathbf{s},\mathbf{r})$, follow Equations (A8) and (A9), respectively.

4.2.2 | Sorting approximate Pareto-optimal solutions

Let Ω_a denote the existing candidate solutions that are the samples of $\mathcal{D}$ at the beginning of the optimization process and are enriched after each optimization iteration, which is discussed later. Among the members of Ω_a, a non-dominated sorting approach[37] seeks a set of approximate Pareto-optimal solutions to problem (16) once $\hat{\beta}(\mathbf{s},\mathbf{r})$, $\hat{\delta}(\mathbf{s},\mathbf{r})$, $\hat{\varphi}(\mathbf{s},\mathbf{r})$, and $\hat{\omega}(\mathbf{s},\mathbf{r})$ have been developed. In this way, $f_2(\mathbf{s})$, $\delta(\mathbf{s})$, $\varphi(\mathbf{s})$, and $\omega(\mathbf{s})$ for each member of Ω_a can be evaluated through the MCS using the mean functions of the corresponding GP models, such that

$$f_2(\mathbf{s}) = -\mathbb{E}\left[\beta(\mathbf{s},\mathbf{r})\right] \approx -\frac{1}{n_r}\sum_{i=1}^{n_r} \mu_{\hat{\beta}(\mathbf{s},\mathbf{r}_i)} \tag{20}$$

$$g(\mathbf{s}) = 1 - \epsilon_{1(2,3)} - \mathbb{P}\left[g(\mathbf{s},\mathbf{r}) \leq 0\right] \approx 1 - \epsilon_{1(2,3)} - \frac{1}{n_r}\sum_{i=1}^{n_r} \mathbb{I}[\mu_{\hat{g}(\mathbf{s},\mathbf{r}_i)} \leq 0] \tag{21}$$

where $g(\mathbf{s})$ is either $\delta(\mathbf{s})$, $\varphi(\mathbf{s})$, or $\omega(\mathbf{s})$; n_r is the number of $\mathbf{r}$ realizations; and $\mathbb{I}[\cdot] = 1$ if $[\cdot]$ is true and $\mathbb{I}[\cdot] = 0$ otherwise. Parallel computing is also carried out to speed up the solution-sorting process.

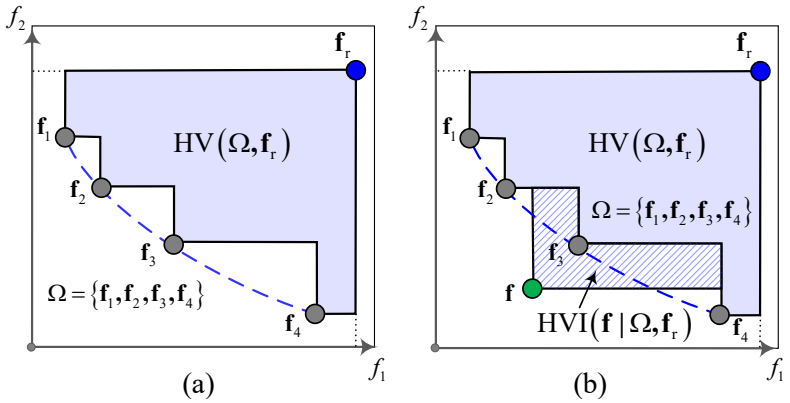

FIGURE 2 Examples of the HV and HVI with two objective functions: (a) HV; (b) HVI.

4.2.3 | Next sampling points of discrete design variables

As the current approximate solutions to problem (16) are found based on the GP models $\hat{\beta}(\mathbf{s},\mathbf{r})$, $\hat{\delta}(\mathbf{s},\mathbf{r})$, $\hat{\varphi}(\mathbf{s},\mathbf{r})$, and $\hat{\omega}(\mathbf{s},\mathbf{r})$, it is desirable to update these solutions by sequentially specifying a promising region of the input variables in which the current solutions and the accuracy of the current GP models are deemed to be improved. It follows that the input variable vectors belonging to such a promising region should have the following three properties: (1) they improve the current solutions considerably; (2) they have a high chance for being feasible solutions to problem (16); and (3) they do not appear in the current training dataset. As the input variable space consists of the spaces of the discrete design variables $\mathbf{s}$ and continuous random parameters $\mathbf{r}$, it is natural to divide the exploration of the promising region into two phases.[12] The first phase, discussed in this section, specifies new sampling vectors of $\mathbf{s}$, denoted as $\mathbf{s}_\mathrm{n}$, which are responsible for the three aforementioned properties. The second phase, discussed in the next section, determines new sampling vectors of $\mathbf{r}$, denoted as $\mathbf{r}_\mathrm{n}$, for addressing the third property.

To improve the current solutions, a hypervolume-based approach by Do et al.[12] is adopted in this study. Let $\Omega=\{\mathbf{f}_1,...,\mathbf{f}_M\}\in\mathbb{R}^k$ and $\mathbf{f}_\mathrm{R}\in\mathbb{R}^k$ denote the current set of M approximate Pareto-optimal solutions in a space of k objective functions and a fixed reference point dominated by all elements of Ω, respectively. Each element of $\mathbf{f}_\mathrm{R}$ may be assigned as the maximum of the corresponding objective function. Ω and $\mathbf{f}_\mathrm{R}$ together define a confined space surrounded by them called hypervolume (HV) indicator measure,[38] which is depicted in Figure 2(a) as an area between a set of four solutions to a bi-objective minimization problem and a reference point dominated by these solutions. In essence, the HV is a Lebesgue measure of the k-dimensional subspace dominated by Ω and bounded above by $\mathbf{f}_\mathrm{R}$, as

$$\mathrm{HV}(\Omega,\mathbf{f}_\mathrm{R})=\Lambda\left(\left\{\mathbf{f}\in\mathbb{R}^k\mid\exists\mathbf{f}_m\in\Omega:\mathbf{f}_m\preceq\mathbf{f}\text{ and }\mathbf{f}\preceq\mathbf{f}_\mathrm{R}\right\}\right)\tag{22}$$

where $\Lambda(\cdot)$ denotes the Lebesgue measure; $\mathbf{f}$ is a point in the k-dimensional space of the objective functions; and $\mathbf{f}_m\preceq\mathbf{f}$ indicates $\mathbf{f}_m$ dominates $\mathbf{f}$. The HV in this study is evaluated using a sampling technique incorporated in the MATLAB function *hypervolume*.[39]

The field of multi-objective design commonly uses the HV to compare different sets of candidate solutions to a multi-objective optimization problem. For two arbitrary sets of solutions, the set with larger HV is better than the other one. Therefore, if each of the new sampling points $\mathbf{s}_\mathrm{n}$ improves the current approximate solutions, the union of the corresponding objective function vector $\mathbf{f}$ and Ω should form a new HV greater than that of the current Ω. This improvement is incorporated in the following hypervolume improvement indicator (HVI).[12]

$$\mathrm{HVI}(\mathbf{f}\mid\Omega,\mathbf{f}_\mathrm{R})=\mathrm{HV}(\mathbf{f}\cup\Omega,\mathbf{f}_\mathrm{R})-\mathrm{HV}(\Omega,\mathbf{f}_\mathrm{R})\tag{23}$$

where $\mathbf{f}\cup\Omega$ denotes the union of $\mathbf{f}$ and Ω. Figure 2(b) shows an example of the HVI for an objective function vector $\mathbf{f}$ and a set of four solutions to a bi-objective minimization problem. The HVI should be maximized for a major improvement in the current HV.

Another important requirement for the vectors $\mathbf{s}_\mathrm{n}$ is that they should have a high chance to become feasible solutions to the problem (16). Accordingly, $\mathbf{s}_\mathrm{n}$ must satisfy the deterministic constraints of problem (12) and belong to a region in which $\delta(\mathbf{s})$, $\varphi(\mathbf{s})$, and $\omega(\mathbf{s})$ are minimized simultaneously. In other words, $\mathbb{P}[\delta(\mathbf{s},\mathbf{r})\le 0]$, $\mathbb{P}[\varphi(\mathbf{s},\mathbf{r})\le 0]$, and $\mathbb{P}[\omega(\mathbf{s},\mathbf{r})\le 0]$ should be

simultaneously maximized, which is further transformed to maximizing the following feasibility indicator (FI).

$$\mathrm{FI}(\mathbf{s}) = \mathbb{P}\left[\delta(\mathbf{s},\mathbf{r}) \le 0\right] \mathbb{P}\left[\varphi(\mathbf{s},\mathbf{r}) \le 0\right] \mathbb{P}\left[\omega(\mathbf{s},\mathbf{r}) \le 0\right] \tag{24}$$

where FI is formulated from the fact that $\delta(\mathbf{s})$, $\varphi(\mathbf{s})$, and $\omega(\mathbf{s})$ are uncorrelated, and $\mathbb{P}\left[\delta(\mathbf{s},\mathbf{r}) \le 0\right]$, $\mathbb{P}\left[\varphi(\mathbf{s},\mathbf{r}) \le 0\right]$, and $\mathbb{P}\left[\omega(\mathbf{s},\mathbf{r}) \le 0\right]$ always take positive values. The FI conflicts with the HVI as its maximizer tends to minimize the HV. It, therefore, is rational to formulate a bi-objective deterministic maximization problem for managing these conflicting criteria.

The last property of the promising region requires that the vectors $\mathbf{s}_\mathrm{n}$ do not belong to the current training dataset $\mathcal{D}$. Thus, $\mathbf{s}_\mathrm{n}$ can be specified after each optimization iteration by solving the following bi-objective deterministic maximization problem.

$$\begin{aligned} \mathbf{s}_\mathrm{n} = \underset{\mathbf{s}\notin\mathcal{D}}{\operatorname{argmax}} \quad & \left[\mathrm{HVI}(\mathbf{f} \mid \Omega, \mathbf{f}_\mathrm{R}), \mathrm{FI}(\mathbf{s})\right] \\ \text{subject to} \quad & g_i(\mathbf{s}) \le 0,\ i = 1,..2d_1 \\ & l_j(\mathbf{s}) \le 0,\ j = 1,..J \\ & s_i \in S_i,\ i = 1,..d_1 \end{aligned} \tag{25}$$

Problem (25) is solved using a non-dominated sorting genetic algorithm (NSGA-II).[37] Parameters characterizing NSGA-II including the population size, maximum number of generations, crossover fraction, tolerance for the objective and constraint functions are 2000, 100, 80%, and 10^{-6}, respectively. Since exact values of FI at $\mathbf{s}_\mathrm{n}$ are not important for solving problem (16), problem (25) can be solved quickly by using a saddlepoint approximation[16] for reasonable estimations of the probabilities incorporated in the FI rather than using the MCS. Solutions to problem (25) are then added to the current training dataset $\mathcal{D}$ and the set Ω_a for updating the current GP models and for sorting the solutions in the next optimization iteration, respectively.

4.2.4 | Next sampling points of correlated random parameters

Once $\mathbf{s}_\mathrm{n}$ have been found, the new sampling points $\mathbf{r}_\mathrm{n}$ of the correlated random parameters are specified accordingly. As previously mentioned, the vectors $\mathbf{r}_\mathrm{n}$ address the last property of the promising region. Thus, they are randomly generated using Equation (19) so that they do not belong to the current training dataset $\mathcal{D}$. The number of $\mathbf{r}_\mathrm{n}$ equals that of $\mathbf{s}_\mathrm{n}$.

4.2.5 | Enrichment of the existing candidate solutions

The set Ω_a of the existing candidate solutions is enriched before starting a new optimization iteration. The enriched Ω_a consists of three different groups of the discrete candidate solutions $\mathbf{s}$. The first group includes the samples of the updated training dataset $\mathcal{D}$ because it is rational to expect that the new sampling points $\mathbf{s}_\mathrm{n}$, which improve the solution quality, become the solutions to problem (16). The second group consists of the new candidates generated by performing a total of k_1 random perturbations (in the design variable space) surrounding each of the current approximate Pareto-optimal solutions of the set Ω, which can be regarded as performing discrete local searches. Each perturbation randomly increases or decreases each integer element of every approximate Pareto-optimal solution by an integer value, such as 1, 2, 3, or 4.[12] Therefore, the random perturbations set an expectation that some improvement in the solutions may be achieved through the discrete local searches in the design variable space of the current solutions even though the neighborhood in this space differs from that in the objective function space. With the same expectation for the solution improvement, the third group consists of a total of k_2 new candidates generated uniformly over the design domain, which can be regarded as performing discrete global searches.

4.3 | Optimization procedure

Figure 3 summarizes the proposed optimization procedure for solving problem (16). Accordingly, the following six steps are executed sequentially and incorporated into an in-house MATLAB function.

- Step 1: Generate samples of $\mathbf{s}$ and $\mathbf{r}$. Then, create the training dataset $\mathcal{D}$ by performing the NRHA for each sample.
- Step 2: Construct GP models to approximate $\beta(\mathbf{s},\mathbf{r})$, $\delta(\mathbf{s},\mathbf{r})$, $\varphi(\mathbf{s},\mathbf{r})$, and $\omega(\mathbf{s},\mathbf{r})$.
- Step 3: Sort the approximate Pareto-optimal solutions among the existing candidate solutions of the set Ω_a.
- Step 4: Terminate the optimization process and output the approximate Pareto-optimal solutions if one of the following stopping criteria is satisfied: (1) the number of optimization iterations reaches an upper limit t_u specified the designer and (2) the relative difference of the HVs at the current and previous iterations is less than or equal to a small positive value α. Otherwise, proceed to Step 5.

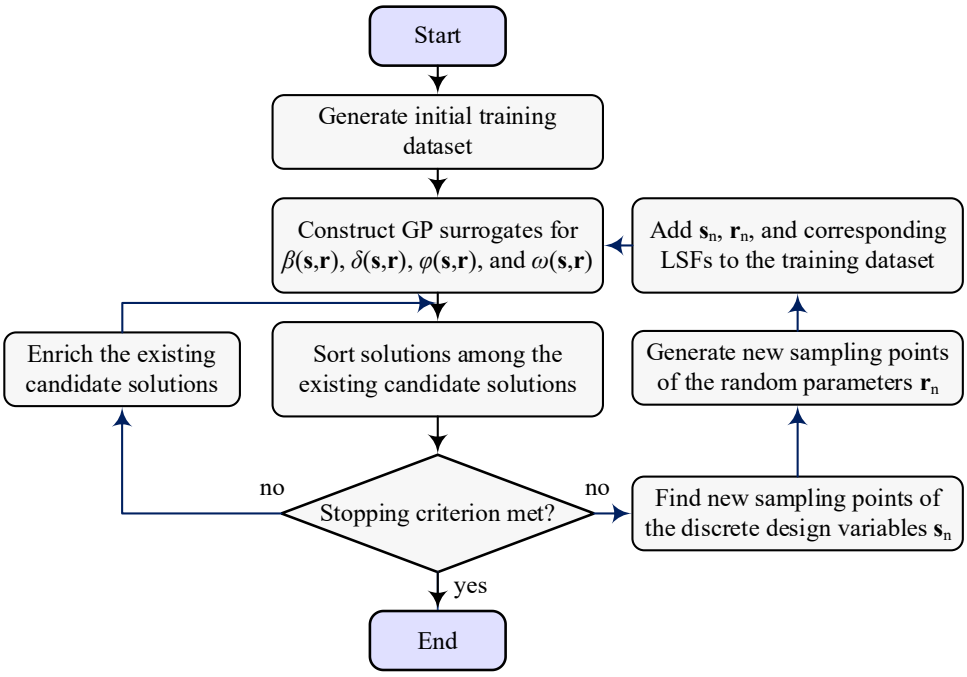

FIGURE 3 Proposed optimization procedure.

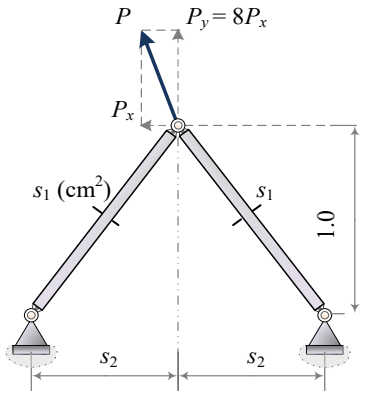

FIGURE 4 Two-bar truss.

- Step 5: Find new sampling points $\mathbf{s}_n$ and $\mathbf{r}_n$. If no new sampling point is found, i.e., problem (25) has no solution, terminate the optimization process. Otherwise, enrich Ω_a and go to Step 6.
- Step 6: Evaluate the LSFs of interest for $\mathbf{s}_n$ and $\mathbf{r}_n$ found in Step 5 using the NRHA; update $\mathcal{D}$ and the current GP models for $\beta(\mathbf{s},\mathbf{r})$, $\delta(\mathbf{s},\mathbf{r})$, $\varphi(\mathbf{s},\mathbf{r})$, and $\omega(\mathbf{s},\mathbf{r})$; and reiterate from Step 3.

5 | TEST PROBLEM

To carefully assess its performance, the proposed optimization method is used for optimizing a two-bar truss as shown in Figure 4, which is taken from Do et al.[12]. Two design variables of the truss are the cross-sectional area s_1 of its members and the horizontal span s_2, i.e., $\mathbf{s} = [s_1, s_2]^T$. The random parameters consist of the magnitude of the external load P, the mass density ρ and yield stress σ_y of the truss material, i.e., $\mathbf{r} = [\rho, P, \sigma_y]^T$. They are assumed to be uncorrelated in this case as

TABLE 2 Random parameters for the two-bar truss.[12]

Parameter	Description	Mean	COV	Distribution
ρ	Mass density [kg/m^3]	10^4	0.20	Lognormal
P	External load [kN]	800	0.25	Lognormal
σ_y	Yield stress [MPa]	1050	0.24	Normal

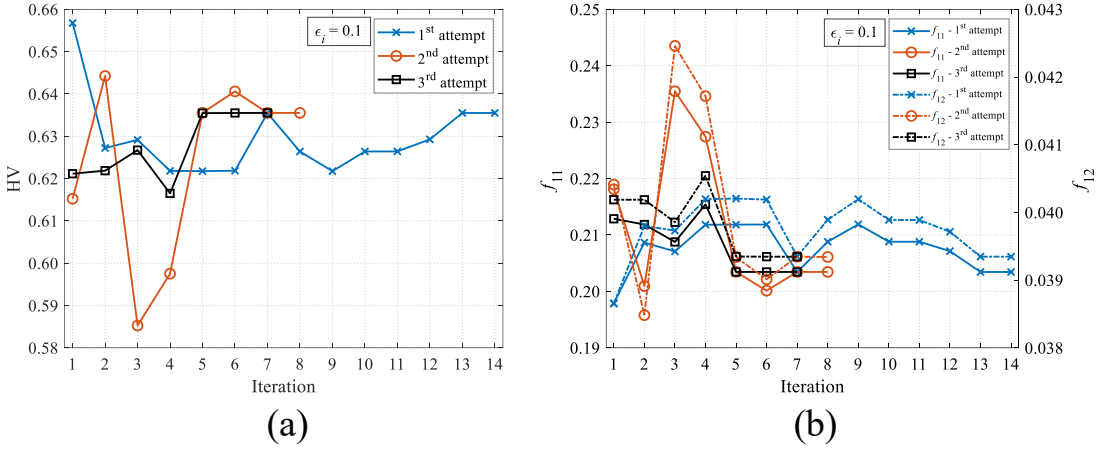

FIGURE 5 Histories of the optimization process for solving the two-bar truss with $\epsilon_i = 0.1$: (a) HV; (b) objective functions.

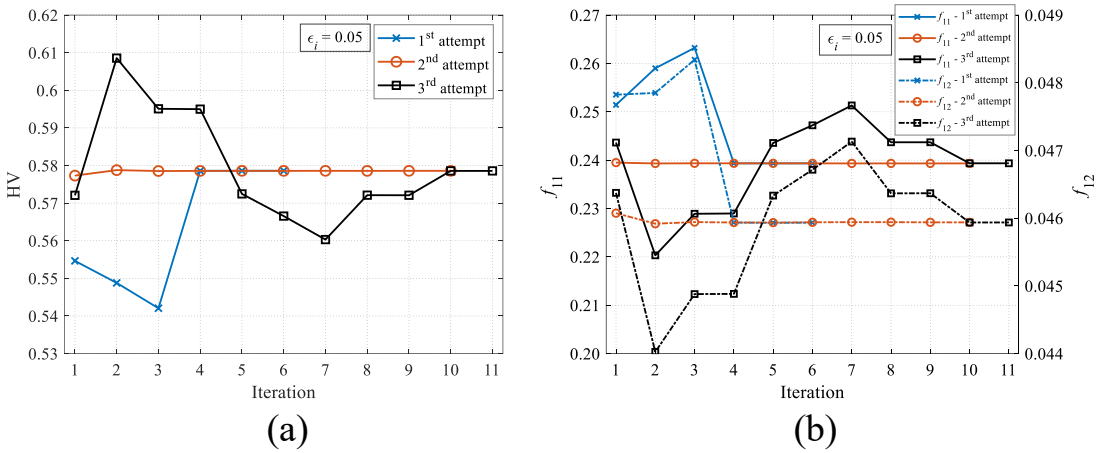

FIGURE 6 Histories of the optimization process for solving the two-bar truss with $\epsilon_i = 0.05$: (a) HV; (b) objective functions.

their correlation coefficients are set as 0. Probabilistic characteristics of $\mathbf{r}$ are provided in Table 2, where COV stands for the coefficient of variation of the parameter.

A bi-objective RBDO problem whose formulation is similar to that of problem (12) or (16) is formulated for the truss. The mean and standard deviation of the total mass of the truss are considered as two objective functions, while the probabilistic constraints are associated with the axial stress in the truss members.[12] Let $f_1(\mathbf{s},\mathbf{r})$ indicate the total mass of the truss, $f_{11}(\mathbf{s}) = \mathbb{E}\left[f_1(\mathbf{s},\mathbf{r})\right]$ and $f_{12}(\mathbf{s}) = \sqrt{\mathrm{var}\left[f_1(\mathbf{s},\mathbf{r})\right]}$ represent the mean and standard deviation of $f_1(\mathbf{s},\mathbf{r})$, respectively. Also, let $g_1(\mathbf{s},\mathbf{r})$ and $g_2(\mathbf{s},\mathbf{r})$ denote the LSFs corresponding to the axial stress in the truss members. For simplification, $g_1(\mathbf{s},\mathbf{r})$ and $g_2(\mathbf{s},\mathbf{r})$ do not

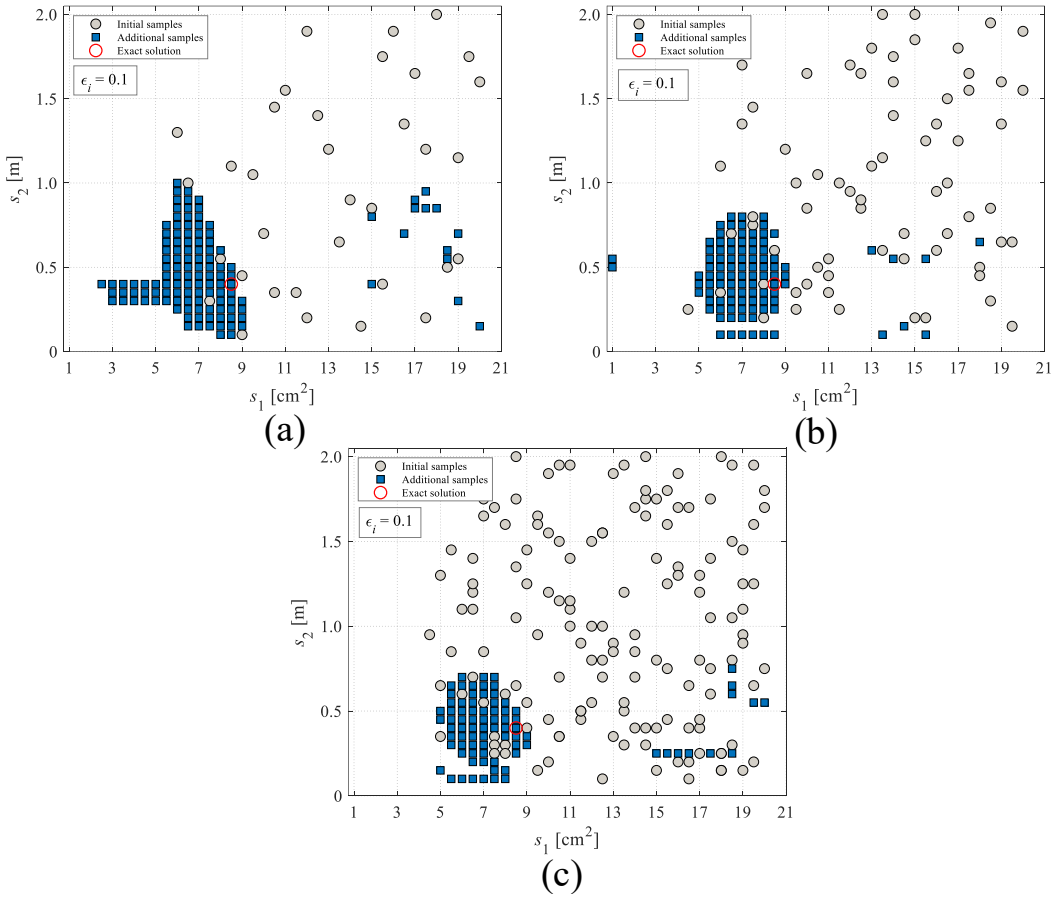

FIGURE 7 Histories of specifying new sampling points of the design variables for the two-bar truss with $\epsilon_i = 0.1$: (a) 1st attempt; (b) 2nd attempt; (c) 3rd attempt.

account for the self-weight of the truss. Thus, the bi-objective RBDO problem of the truss is stated as follows:

$$\begin{aligned} \min_{\mathbf{s}} . \quad & \left[f_{11}(\mathbf{s}), f_{12}(\mathbf{s})\right] \\ \text{subject to} \quad & \mathbb{P}\left[g_1(\mathbf{s},\mathbf{r}) \le 0\right] \ge 1-\epsilon_1 \\ & \mathbb{P}\left[g_2(\mathbf{s},\mathbf{r}) \le 0\right] \ge 1-\epsilon_2 \\ & s_1 \in \mathcal{S}_1 = \{1.0, 1.5, \ldots, 20.0\}\text{cm}^2 \\ & s_2 \in \mathcal{S}_2 = \{0.1, 0.15, \ldots, 2.0\}\text{m} \end{aligned} \tag{26}$$

where $\mathcal{S}_1$ and $\mathcal{S}_2$ are design sets for selecting s_1 and s_2, respectively, and

$$f_1(\mathbf{s},\mathbf{r}) = \frac{10^{-4}\rho s_1\sqrt{1+s_2^2}}{m_{\max}} \tag{27}$$

$$g_1(\mathbf{s},\mathbf{r}) = \frac{5P}{\sqrt{65}s_1\sigma_y}\sqrt{1+s_2^2}\left(8+\frac{1}{s_2}\right) - 1 \tag{28}$$

$$g_2(\mathbf{s},\mathbf{r}) = \frac{5P}{\sqrt{65}s_1\sigma_y}\sqrt{1+s_2^2}\left(8-\frac{1}{s_2}\right) - 1 \tag{29}$$

Here $m_{\max} = 45$ kg is the maximum nominal mass of the truss.

As $f_1(\mathbf{s},\mathbf{r})$ is a linear function of ρ, $f_{11}(\mathbf{s})$ can be derived as $f_{11}(\mathbf{s}) = \left(\mathbb{E}[\rho]/\sqrt{\text{var}[\rho]}\right) f_{12}(\mathbf{s}) = 5f_{12}(\mathbf{s})$. Therefore, the set of Pareto-optimal solutions to problem (26) has only one solution.

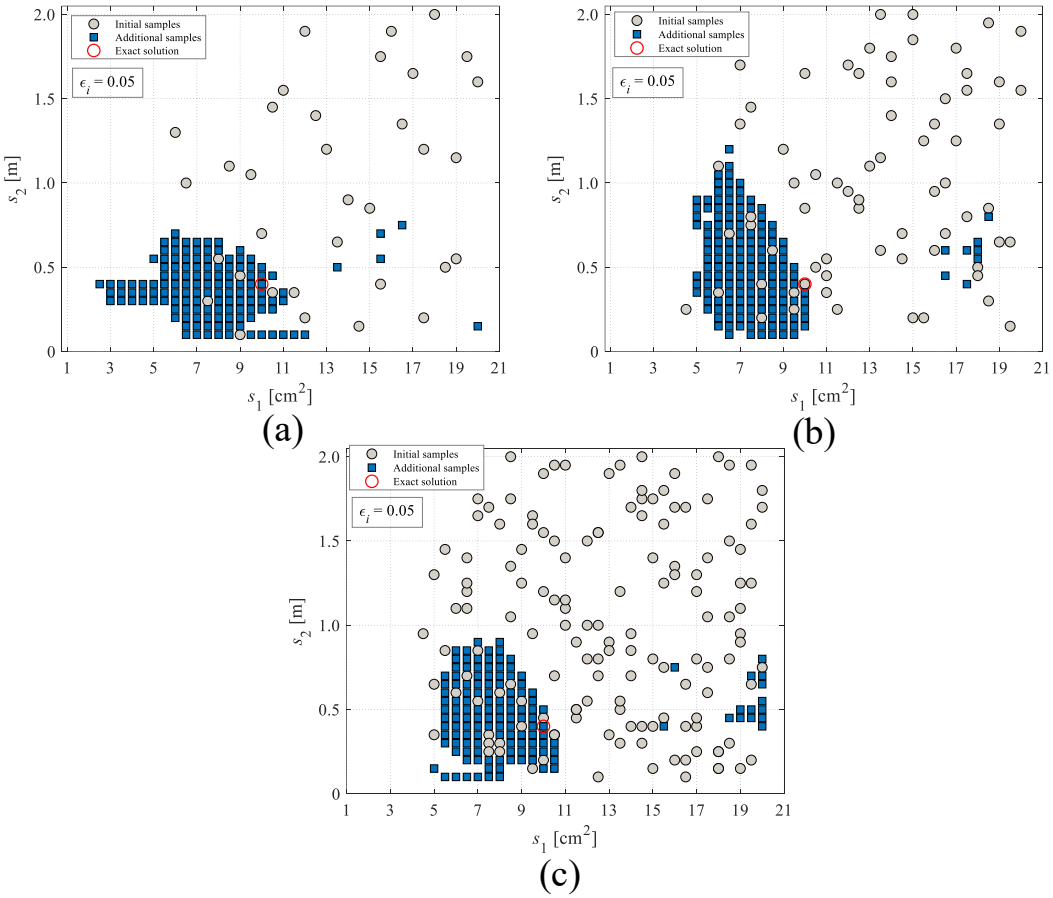

FIGURE 8 Histories of specifying new sampling points of the design variables for the two-bar truss with $\epsilon_i = 0.05$: (a) 1st attempt; (b) 2nd attempt; (c) 3rd attempt.

To examine the robustness of the proposed method, three different training datasets are generated for processing optimization of the truss. The first, second, and third training datasets having 50, 100, and 200 samples of the input variables, respectively, are used for calculating $f_1(\mathbf{s}, \mathbf{r})$, $g_1(\mathbf{s}, \mathbf{r})$, and $g_2(\mathbf{s}, \mathbf{r})$. However, only 34, 69, and 143 samples offering non-positive values of $f_1(\mathbf{s}, \mathbf{r})$, $g_1(\mathbf{s}, \mathbf{r})$, and $g_2(\mathbf{s}, \mathbf{r})$ serve as the feasible training samples. To develop the GP models for $f_1(\mathbf{s}, \mathbf{r})$, $g_1(\mathbf{s}, \mathbf{r})$, and $g_2(\mathbf{s}, \mathbf{r})$, the DACE toolbox[40] is used together with a first-degree-polynomial mean function; see Appendix. It is desirable to validate the accuracy of the GP models against a test dataset if only one set of the models is used throughout the optimization process. However, it is not necessary to do so in this study because the GP models are updated sequentially during the optimization process. In the proposed optimization method, the accuracy of the GP models is refined intelligently in the promising region of the input variable space and therefore, the improvement in the solutions indicates the improvement in the GP models in such a region.

Problem (26) is solved for two risk levels $\epsilon_i = 0.1$ and 0.05 ($i = 1, 2$). For each risk level, the optimization process is carried out three times corresponding to the three training datasets. In each optimization iteration, the MCS uses $n_r = 4 \times 10^4$ samples of $\mathbf{r}$ for evaluating the objective and probabilistic constraint functions. To update Ω_a, set $k_1 = 100$ and $k_2 = 500$. The reference point is specified as $\mathbf{f}_R = [1, 0.2]^T$. The stopping criteria include $t_u = 20$ iterations and $\alpha = 10^{-9}$.

Figures 5 and 6 show histories of the optimization process for $\epsilon_i = 0.1$ and 0.05, respectively. Although the evolution of the HV and that of the objective functions for the three optimization trials of each risk level follow different patterns due to the use of different training datasets, the optimization process is still able to quickly terminate and provides a unique solution. The designs of the truss for $\epsilon_i = 0.1$ and 0.05 are $\mathbf{s} = [8.5, 0.4]^T$ and $[10.0, 0.4]^T$, respectively. The maximum computational times required for $\epsilon_i = 0.1$ and 0.05 are 5257 and 4058 s using an Intel(R) i7-1165G7 2.80 GHz CPU and 8.0 GB memory, respectively.

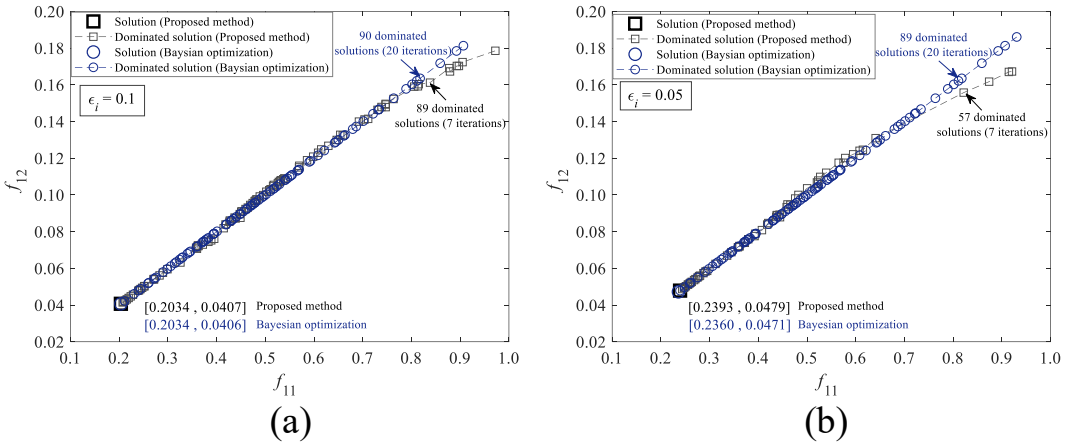

FIGURE 9 Comparison of optimization results for the two-bar truss by the proposed method and by Bayesian optimization: (a) $\epsilon_i = 0.1$; (b) $\epsilon_i = 0.05$.

TABLE 3 Comparison of optimization results for the two-bar truss.

Variable/objective	$\epsilon_1 = \epsilon_2 = 0.1$				$\epsilon_1 = \epsilon_2 = 0.05$			
	1st	2nd	3rd	Exact	1st	2nd	3rd	Exact
s_1 [cm^2]	8.5	8.5	8.5	8.5	10.0	10.0	10.0	10.0
s_2 [m]	0.40	0.40	0.40	0.40	0.40	0.40	0.40	0.40
f_{11}	0.2034	0.2001	0.2034	0.2033	0.2393	0.2393	0.2394	0.2397
f_{12}	0.0407	0.0400	0.0407	0.0407	0.0479	0.0479	0.0479	0.0480

Figures 7 and 8 provide histories of specifying the new sampling points $\mathbf{s}_\mathrm{n}$ during the optimization process for $\epsilon_i = 0.1$ and 0.05, respectively. As is clear, the new sampling points $\mathbf{s}_\mathrm{n}$ tend to distribute in the neighborhood of the exact solution to problem (27), leading to quick termination of the optimization process as observed.

To further verify the obtained designs, exact solution to problem (26) is found for each risk level. Since both $\mathcal{S}_1$ and $\mathcal{S}_1$ have 39 elements, a total of $39 \times 39 = 1521$ possible designs can be specified for the truss. A total of 10^5 samples of $\mathbf{r}$ are also generated for evaluating $f_{11}(\mathbf{s})$, $f_{12}(\mathbf{s})$, $\mathbb{P}\left[g_1(\mathbf{s},\mathbf{r}) \le 0\right]$, and $\mathbb{P}\left[g_2(\mathbf{s},\mathbf{r}) \le 0\right]$ associated with each design. In this way, the exact solution can be sorted for each risk level. Table 3 indicates a good agreement between the designs by the proposed method and the exact ones. Furthermore, the performance of the proposed method is compared with that of a Bayesian optimization method.[12] Figure 9 shows that the proposed method outperforms the Bayesian optimization in terms of the numbers of optimization iterations and generated feasible solutions.

6 | DESIGN EXAMPLE

This section investigates a six-story two-bay frame as shown in Figure 10(a). The frame is considered as a lateral load resisting system for a residential building. The site soil is assumed to be stiff as the property of site class D according to ASCE 7-16.[4] Parameters for the mapped MCER, 5%-damped, spectral response acceleration involve $T_\mathrm{S} = 1.250$g and $S_1 = 0.4$g. The long-period transition period is $T_\mathrm{L} = 10$ s.

The design ground motions are evaluated using an upper bound value of the fundamental natural period of the frame $T = 1.2$ s, which is derived from equation (12.8-7) of ASCE 7-16.[4] Once the preliminary design of the frame is specified, the nominal value of its fundamental natural period can be evaluated and that should not exceed 1.2 s.

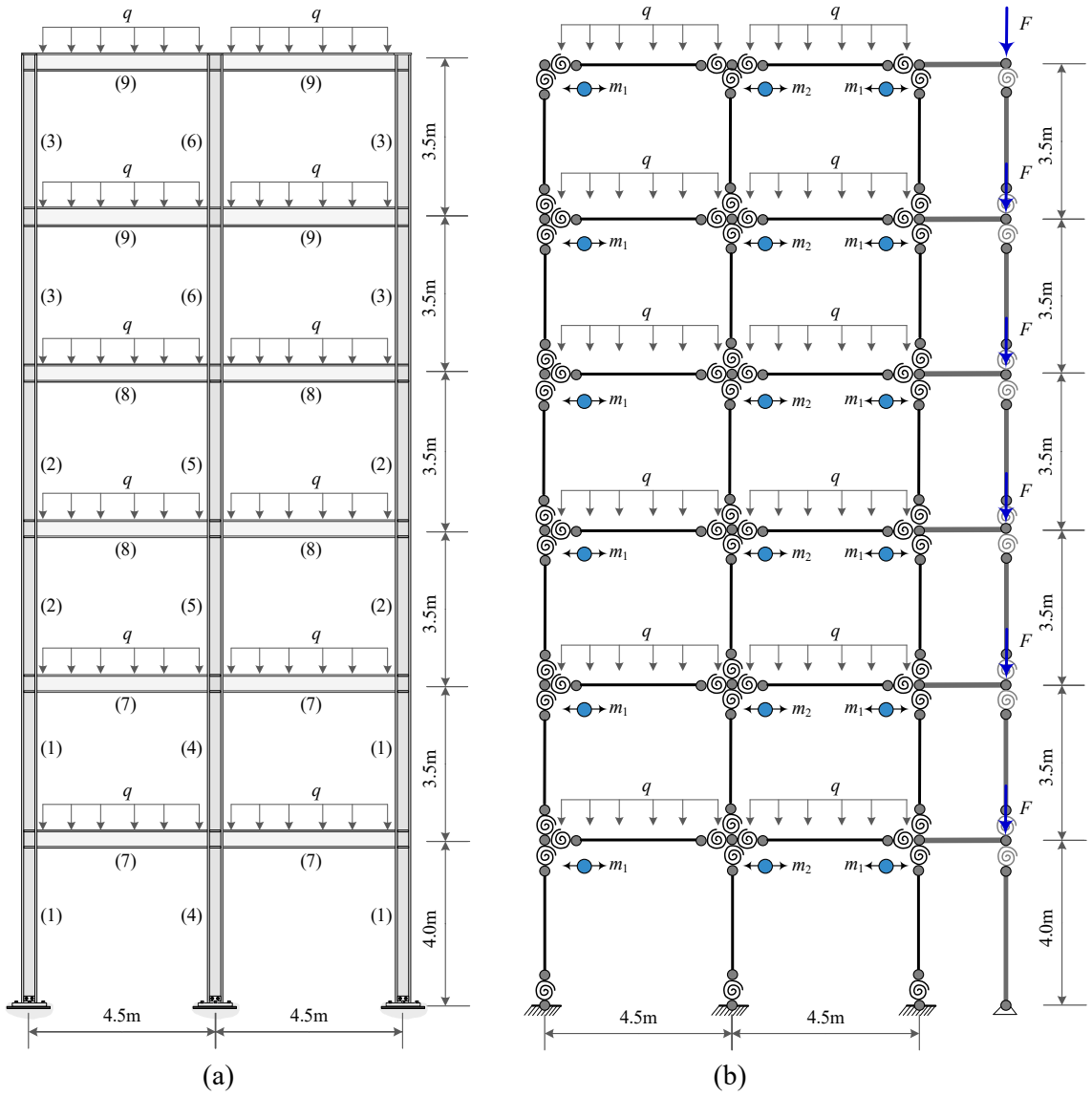

FIGURE 10 Six-story two-bay frame (a) and its finite element model (b).

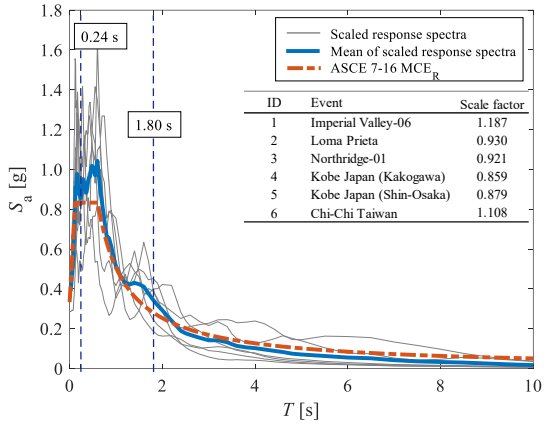

FIGURE 11 Comparison of the mean, 5%-damped response spectrum of scaled ground motions with ASCE 7-MCE$_R$ spectrum.

TABLE 4 List of sections of columns and beams for the frame.

ID	Column $S_{1,\ldots,6}$	$\rho_{1,\ldots,6}$ [kg/m]	Beam $S_{7,8,9}$	$\rho_{7,8,9}$ [kg/m]
1	W16×77	114.0	W24×55	82.0
2	W16×67	100.0	W21×57	85.0
3	W14×82	122.0	W21×55	82.0
4	W14×74	110.0	W21×50	74.0
5	W14×68	101.0	W18×65	97.0
6	W14×61	91.0	W18×60	89.0
7	W14×53	79.0	W18×40	60.0
8	W14×48	72.0	W18×35	52.0
9	W12×58	86.0	W16×57	85.0
10	W12×53	79.0	W16×50	75.0
11	W12×50	74.0	W16×45	67.0
12	W12×45	67.0	W16×40	60.0
13	W10×54	80.0	W14×61	91.0
14	W10×49	73.0	W14×53	79.0
15	W10×45	67.0	W14×48	72.0
16	W8×40	59.0	W14×38	57.8
17	W8×35	52.0	W14×34	51.0
18	W8×31	46.1	W14×30	44.0

TABLE 5 Random parameters for the frame.

Parameter	Description	Mean	COV	Distribution
q	Distributed mass [t/m]	3.06	0.20	Normal
F	Gravity load [kN]	500	0.10	Normal
E	Young's modulus [GPa]	200	0.04	Normal
σ_y	Yield stress [MPa]	262.50	0.06	Normal
θ_p	Pre-capping plastic rotation [rad]	0.022	0.27	Lognormal*
θ_{pc}	Post-capping plastic rotation [rad]	0.17	0.35	Lognormal*
θ_u	Ultimate rotation capacity [rad]	0.06	–	–
λ	Reference cumulative rotation capacity [rad]	1.10	0.44	Lognormal*
M_c/M_y	Post-yield strength ratio	1.11	0.05	Normal
κ	Residual strength ratio	0.40	0.10	Normal

* Mean and standard deviation of logarithmic value

The scale factor for each selected ground motion in Table 1 and the associated scaled acceleration spectrum are given in Figure 11. The design acceleration history of each ground motion is determined by multiplying the recorded acceleration history by the corresponding scale factor.

6.1 | Numerical model

The frame has 30 members classified into six column groups, i.e., groups (1) to (6), and three beam groups, i.e., groups (7), (8), and (9). Possible steel sections for the members in each group are given in Table 4.

The OpenSees[41] is used to develop a numerical model for the frame, as shown in Figure 10(b). In this model, a leaning column with gravity load F is linked to the frame at each floor by a rigid truss element to account for P-Δ effects, where F

TABLE 6 Correlation coefficients for the random parameters[23].

	E	σ_y	θ_p	θ_{pc}	λ
E	1.00	0.71	0	0	0
σ_y	0.71	1.00	0	0	0
θ_p	0	0	1.00	0.69	0.44
θ_{pc}	0	0	0.69	1.00	0.67
λ	0	0	0.44	0.67	1.00

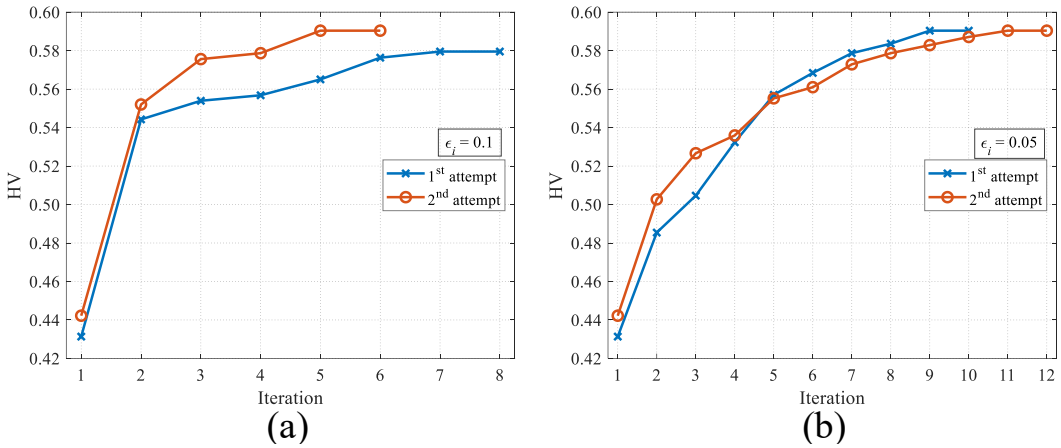

FIGURE 12 Histories of the HVs by different optimization trials for the frame with two risk levels: (a) $\epsilon_i = 0.1$; (b) $\epsilon_i = 0.05$.

TABLE 7 Comparisons of the energy dissipation ratios of beam members and the uncertain constraints between different selected designs of the frame.

Design	Objective or constraint	$\epsilon_1 = \epsilon_2 = \epsilon_3 = 0.1$		$\epsilon_1 = \epsilon_2 = \epsilon_3 = 0.05$	
		Proposed method	NRHA	Proposed method	NRHA
$\mathbf{s}_1$	$f_2(\mathbf{s}_1)$	0.808	0.819	0.806	0.808
	$\delta(\mathbf{s}_1), \varphi(\mathbf{s}_1), \omega(\mathbf{s}_1)$	−0.1	−0.1	−0.05	−0.05
$\mathbf{s}_2$	$f_2(\mathbf{s}_2)$	0.847	0.854	0.844	0.859
	$\delta(\mathbf{s}_2), \varphi(\mathbf{s}_2), \omega(\mathbf{s}_2)$	−0.1	−0.1	−0.05	−0.05

vertically acts on a generic floor of the building for producing overturning action and secondary internal forces to the frame members through the inter-story drift. The leaning column is modeled using a rigid elastic beam-column element connected by two rotational springs with very small rotational stiffness. Also, geometric nonlinearity is considered in structural analysis.

The distributed mass q from the floor acting on each beam member is divided into two equal parts assigned to the end nodes of the element; see Figure 10(b). The mass of each structural member is also assigned to the end nodes of the corresponding element. Thus, the lumped masses m_1 and m_2 in the earthquake direction, as depicted in Figure 10(b), are derived from the masses of the connecting structural members, q, and F. The probabilistic characteristics of q and F are assumed as provided in Table 5. Furthermore, the Rayleigh damping matrix is formulated based on a linear combination of the mass and stiffness matrices. The damping coefficients are calculated by using 5% damping ratio for the first two modes of the frame. The stiffness damping coefficient due to the use of the elastic beam-column element with rotational springs at both ends is also modified according to Equation (9) of the work by Zareian and Medina.[33] The time increment for the NRHA is 0.01 s.

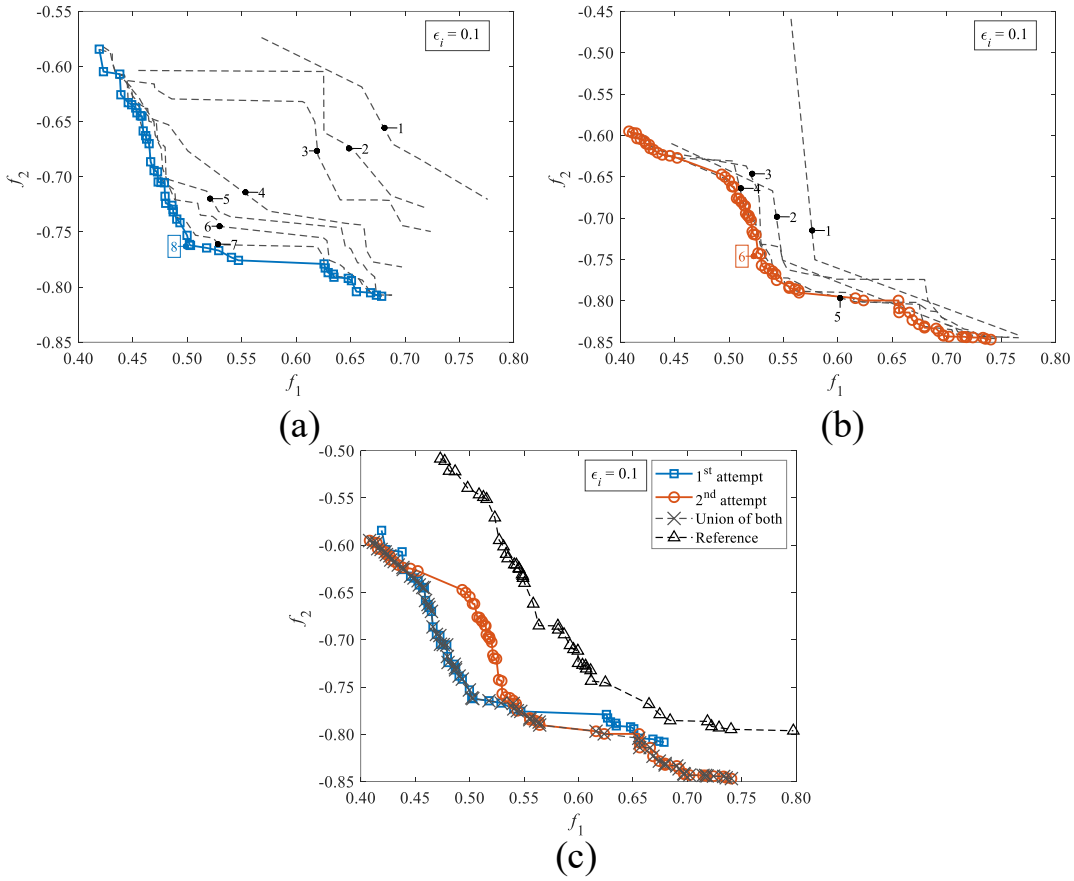

FIGURE 13 Histories of approximate Pareto-optimal solutions for the frame with $\epsilon_i = 0.1$: (a) 1st attempt; (b) 2nd attempt; (c) Comparison of solutions by the two attempts and the reference ones.

6.2 | Random parameters for deterioration model

As described in Section 2.1, the material properties for the modified IK deterioration model include the Young's modulus E; the yield stress σ_y; the rotation capacities θ_p, θ_{pc}, and θ_u ; the reference cumulative rotation capacity λ; and the strength ratios M_c/M_y and κ. The yield rotation θ_y is directly evaluated from E, σ_y, and the section modulus. The probabilistic characteristics of these material parameters and their correlations are taken from the works by Lignos and Krawinkler[31] and Liu et al.[23], as listed in Tables 5 and 6, respectively.

6.3 | Optimization results

Problem (16) is formulated for the frame with two risk levels $\epsilon_i = 0.1$ and 0.05 ($i = 1, 2, 3$). The limit of the inter-story drift ratios is $\delta_a = 2\%$. The allowable plastic rotation angles for the columns and beams are assigned as $\varphi_a = 0.002$ rad and $\omega_a = 0.015$ rad, respectively. The objective function f_1 for the frame is

$$f_1(\mathbf{s}) = \frac{15\rho_1 + 14(\rho_2 + \rho_3) + 7.5\rho_4 + 7(\rho_5 + \rho_6) + 18(\rho_7 + \rho_8 + \rho_9)}{m_{max}} \tag{30}$$

where ρ_i ($i = 1, \ldots, 9$) and $m_{max} = 13107$ kg are selected and derived from the list of sections in Table 4, respectively.

Two different training datasets are generated for performing the optimization process. The first and second datasets having 500 and 1000 feasible sampling points of the input variables, respectively, are used as inputs of the NRHA for evaluating $\beta(\mathbf{s}, \mathbf{r})$, $\delta(\mathbf{s}, \mathbf{r})$, $\varphi(\mathbf{s}, \mathbf{r})$, and $\omega(\mathbf{s}, \mathbf{r})$.

For each risk level, the optimization process is performed two times corresponding to the two training datasets using a PC with an Intel(R) Xeon(R) E5-2643V4 3.40 GHz CPU and 64 GB memory. $f_2(\mathbf{s})$, $\delta(\mathbf{s})$, $\varphi(\mathbf{s})$, and $\omega(\mathbf{s})$ are evaluated for each

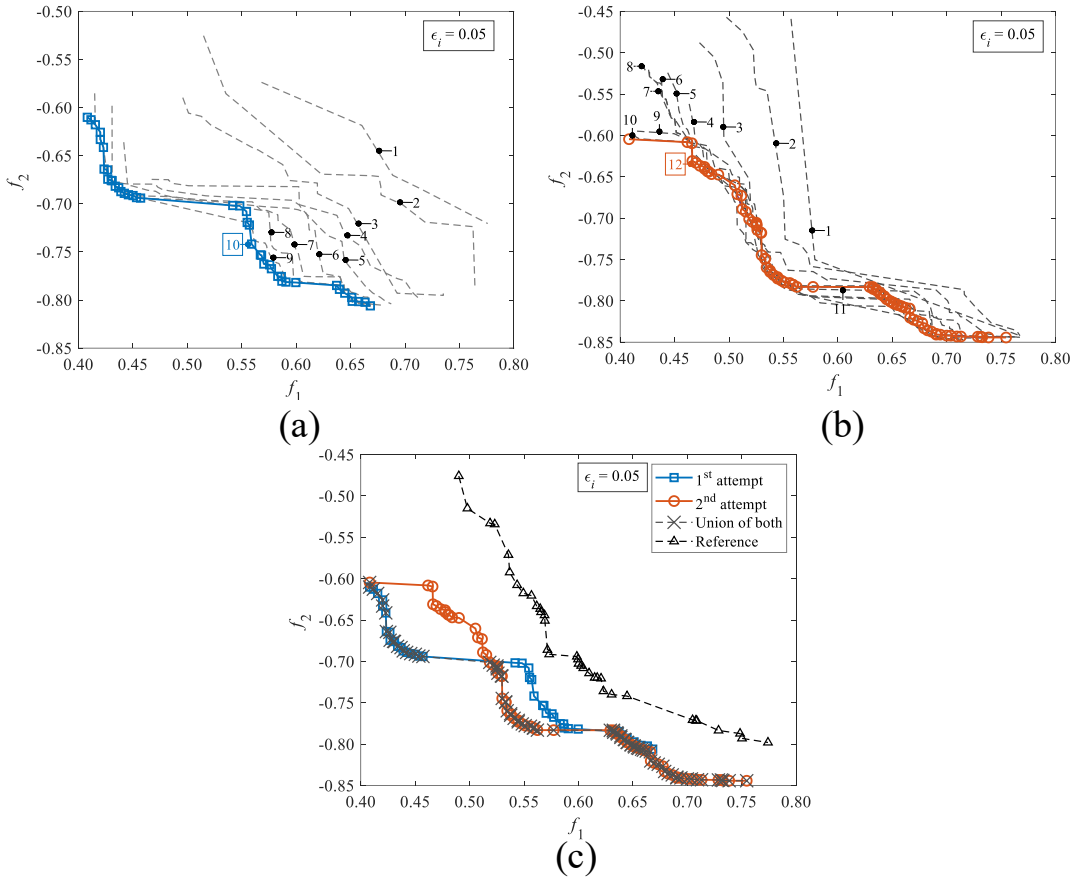

FIGURE 14 Histories of approximate Pareto-optimal solutions for the frame with $\epsilon_i = 0.05$: (a) 1st attempt; (b) 2nd attempt; (c) Comparison of solutions by the two attempts and the reference ones.

candidate solution using a total of $n_r = 4 \times 10^4$ samples of $\mathbf{r}$. To update Ω_a, k_1 and k_2 are set as 200 and 1000, respectively. The reference point and stopping criteria for the optimization process are $\mathbf{f}_R = [1, 0]^T$, $t_u = 20$ iterations, and $\alpha = 10^{-9}$, respectively. Furthermore, the obtained solutions are compared with reference solutions that are found by performing NSGA-II without sequential framework and with the GP models for $\beta(\mathbf{s}, \mathbf{r})$, $\delta(\mathbf{s}, \mathbf{r})$, $\varphi(\mathbf{s}, \mathbf{r})$, and $\omega(\mathbf{s}, \mathbf{r})$ constructed based upon a total of 1000 training samples and the probabilistic constraints evaluated using the saddlepoint approximation.[16]

Figures 12(a) and (b) show the HV histories by the two optimization trials for $\epsilon_i = 0.1$ and 0.05, respectively. The HVs are considerably improved in the very first optimization iterations and gradually increased in the later ones. For each risk level, the final HV corresponding to the second training dataset is slightly greater than that associated with the first one. Notably, the approximate Pareto-optimal solutions are always found for each risk level as the corresponding HV converges.

Figures 13 and 14 compare the obtained solutions by the two optimization trials for $\epsilon_i = 0.1$ and 0.05, respectively. It is clear that the solution quality is guaranteed to improve after each optimization iteration. The Pareto fronts for each risk level by the two optimization trials are different due to the use of different initial training datasets and the randomness of the proposed optimization method. However, the Pareto front can be improved by taking the union of solutions by both trials, as shown in Figures 13(c) and 14(c). More interestingly, the obtained solutions for each risk level completely dominate the corresponding reference solutions, which highlights the importance of the proposed refinement scheme. For $\epsilon_i = 0.1$, the numbers of solutions by the first and second optimization trials are 45 and 69, respectively, and those for $\epsilon_i = 0.05$ are 43 and 82, respectively. The computational times required for the first and second trials with $\epsilon_i = 0.1$ are 8.22 and 12.03 hours, respectively, and those with $\epsilon_i = 0.05$ are 9.88 and 16.52 hours, respectively.

As it is impossible to find the global solutions to problem (16), it is not known whether the solutions obtained by the proposed method are the best optimal ones. Here, the proposed method can only provide the best solutions for a particular setting of the initial training dataset and tuning parameters because the solutions are always found when their quality can no longer be

improved. This is analogous with gradient-based algorithms in the field of structural optimization, which are always guaranteed to converge to a local solution. It, therefore, is desirable to perform optimization several times with different settings of the algorithm so that the best solutions among those from the attempts can be found.

6.4 | Selection of preliminary design

From the Pareto front for each risk level, the solution with maximum energy dissipation ratio of the beams is assigned as the preliminary design of the frame. In this way, the designs corresponding to the first and second optimization trials for $\epsilon_i = 0.1$ are $\mathbf{s}_1 = [2, 6, 6, 1, 2, 4, 18, 8, 18]^T$ and $\mathbf{s}_2 = [2, 2, 3, 3, 5, 12, 15, 17, 18]^T$, respectively, and those for $\epsilon_i = 0.05$ are $\mathbf{s}_1 = [2, 9, 9, 3, 6, 6, 18, 8, 18]^T$ and $\mathbf{s}_2 = [2, 2, 3, 4, 4, 11, 15, 18, 18]^T$, respectively.

To verify the feasibility of these designs, the nominal fundamental natural period, mean of the energy dissipation of the beams, and uncertain LSFs corresponding to each design are evaluated using the NRHA with 1000 samples of $\mathbf{r}$. As a result, the nominal fundamental natural period values corresponding to $\mathbf{s}_1$ and $\mathbf{s}_2$ for $\epsilon_i = 0.1$ are 1.04 and 1.08 s, respectively, and those for $\epsilon_i = 0.05$ are 1.09 and 1.09 s, respectively, which are all less than 1.2 s. The expected energy dissipation ratio of the beams and uncertain constraint functions associated with each design by the proposed method agree with those evaluated by the NRHA, as shown in Table 7. The preliminary designs are feasible as the corresponding probabilistic constraints provide safety margins.

7 | CONCLUSIONS

A novel sequential sampling approach has been presented for solving a discrete bi-objective RBDO problem of moment-resisting steel frames subjected to earthquake excitation. The problem is formulated to optimize the total mass of the frame and energy dissipation of the beam members under unfavorable effects of correlated random parameters of floor masses, external loads, and material properties. The probabilities of exceeding allowable values of both the maximum inter-story drift and the rotational angles of the structural members are constrained, while the compactness of the steel sections is required for fully sustaining plastic deformations. Main conclusions of this work are summarized as follows:

1. Approximations of the dynamic responses using the corresponding GP models facilitate solving the bi-objective RBDO problem of the frame, which may be computationally intractable if the NRHA is directly used for uncertainty propagation.

2. A quick termination and the robustness of the proposed method arise from the fact that the new sampling points of the design variables to refine the accuracy of the GP models tend to distribute in the neighborhood of the exact solutions to the RBDO problem. In other words, the bi-objective deterministic maximization problem formulated for specifying the new sampling points of the proposed refinement scheme is suitable for sequentially solving the RBDO problem.

3. The approximate solutions to the RBDO problem are always found once their quality can no longer be improved, regardless of using a very small number of 10^{-9} as the termination condition on the change in the solution quality and considering the maximum number of optimization iterations as another stopping criterion for the proposed method.

A nontrivial extension to this study is to incorporate uncertainty in the earthquake ground motions and damping ratio into the design optimization process. The serviceability, repairability, and ultimate limit state verifications should be carried out for the frame under different seismic intensities. An optimization problem formulated for both correlated and uncorrelated probabilistic constraints on different collapse mechanisms may also be the focus of future work so that system reliability of the structure can be assessed.

The proposed optimization method can be extended to solving either continuous multi-objective or discrete/continuous single-objective RBDO problems. For continuous multi-objective RBDO problems, Gaussian local searches[42] may be employed for enrichment of the existing candidate solutions instead of the random perturbations as presented in this study. For discrete/continuous single-objective RBDO problems, the so-called expected improvement criterion[43] may be a viable choice to replace the HVI in problem (25).

ACKNOWLEDGMENTS

This work was supported by the JICA AUN/SEED-Net project and by JSPS KAKENHI under Grant Number JP19H02286.

DATA AVAILABILITY STATEMENT

The data that support the findings of this study are available from the corresponding author upon reasonable request.

ORCID

Bach Do https://orcid.org/0000-0002-7359-0668
Makoto Ohsaki https://orcid.org/0000-0003-4935-8874

APPENDIX

A GAUSSIAN PROCESS

Consider the training dataset $\mathcal{D} = \{\mathbf{X}, \mathbf{y}\} = \{\mathbf{x}_i, y_i\}_{i=1}^N$, where $\mathbf{x}_i = [\mathbf{s}_i^T, \mathbf{r}_i^T]^T \in \mathbb{R}^d$ $(d = d_1 + d_2)$ and $y_i \in \mathbb{R}$. The relationship between $\mathbf{x}$ and y is described by $y = \hat{g}(\mathbf{x}) : \mathbb{R}^d \to \mathbb{R}$, where $\hat{g}(\mathbf{x})$ is a Gaussian conditioned on $\mathcal{D}$.

A GP assumes that any finite subset of an infinite set of the output variables y_i has a joint Gaussian distribution.[44] Thus, for N input variable vectors $\mathbf{X} = \{\mathbf{x}_1, \ldots, \mathbf{x}_N\}$, the distribution of the corresponding output variables $\mathbf{y} = \{y_1, \ldots, y_N\}$ follows

$$\begin{bmatrix} y_1 \\ \vdots \\ y_N \end{bmatrix} \sim \mathcal{N}_N \left(\begin{bmatrix} m(\mathbf{x}_1) \\ \vdots \\ m(\mathbf{x}_N) \end{bmatrix}, \begin{bmatrix} k(\mathbf{x}_1, \mathbf{x}_1) & \cdots & k(\mathbf{x}_1, \mathbf{x}_N) \\ \vdots & \ddots & \vdots \\ k(\mathbf{x}_N, \mathbf{x}_1) & \cdots & k(\mathbf{x}_N, \mathbf{x}_N) \end{bmatrix} \right) \tag{A1}$$

where $\mathcal{N}_N$ denotes an N-variate Gaussian, and $m(\mathbf{x})$ and $k(\mathbf{x}, \mathbf{x}')$ are the mean and covariance kernel functions, respectively. $k(\mathbf{x}, \mathbf{x}')$ defined for any pair of $\mathbf{x}$ and $\mathbf{x}'$ measures the similarity between $y = \hat{g}(\mathbf{x})$ and $y = \hat{g}(\mathbf{x}')$, such that

$$k(\mathbf{x}, \mathbf{x}') = \mathbb{E}\left[\left(\hat{g}(\mathbf{x}) - m(\mathbf{x}) \right) \left(\hat{g}(\mathbf{x}') - m(\mathbf{x}') \right) \right] \tag{A2}$$

The following Gaussian kernel function is used in this study.

$$k(\mathbf{x}, \mathbf{x}') = \exp\left(-\frac{(\mathbf{x} - \mathbf{x}')^T (\mathbf{x} - \mathbf{x}')}{2l^2} \right) \tag{A3}$$

where l denotes the characteristic length-scale parameter, determined by using the maximum likelihood estimation of $\mathcal{D}$.[44]

Once l has been found, one wishes to predict the output value y^* for a new input variable vector $\mathbf{x}^*$, i.e., $y^*|\mathbf{y} = \hat{g}(\mathbf{x}^*)$, using the information in Equation (A1). As the GP's nature, the joint PDF of y^* and $\mathbf{y}$ also follows a Gaussian, as

$$\begin{bmatrix} y^* \\ \mathbf{y} \end{bmatrix} \sim \mathcal{N}_{N+1} \left(\begin{bmatrix} m(\mathbf{x}^*) \\ \mathbf{m}(\mathbf{X}) \end{bmatrix}, \begin{bmatrix} k(\mathbf{x}^*, \mathbf{x}^*) & \mathbf{K}(\mathbf{x}^*, \mathbf{X}) \\ \mathbf{K}(\mathbf{x}^*, \mathbf{X})^T & \mathbf{K}(\mathbf{X}, \mathbf{X}) \end{bmatrix} \right) \tag{A4}$$

where $\mathbf{m}(\mathbf{X}) = [m(\mathbf{x}_1), \ldots, m(\mathbf{x}_N)]^T$ and

$$\mathbf{K}(\mathbf{x}^*, \mathbf{X}) = \left[k(\mathbf{x}^*, \mathbf{x}_1), \ldots, k(\mathbf{x}^*, \mathbf{x}_N) \right] \tag{A5}$$

$$\mathbf{K}(\mathbf{X}, \mathbf{X}) = \begin{bmatrix} k(\mathbf{x}_1, \mathbf{x}_1) & \cdots & k(\mathbf{x}_1, \mathbf{x}_N) \\ \vdots & \ddots & \vdots \\ k(\mathbf{x}_N, \mathbf{x}_1) & \cdots & k(\mathbf{x}_N, \mathbf{x}_N) \end{bmatrix} \tag{A6}$$

Therefore, the PDF of the conditional Gaussian $y^*|\mathbf{y} = \hat{g}(\mathbf{x}^*)$ can be derived from Equation (A4) using the standard conditioning rule, such that

$$y^*|\mathbf{y} = \hat{g}(\mathbf{x}^*) \sim \mathcal{N}\left(\mu_{y^*}(\mathbf{x}^*), \sigma_{y^*}^2(\mathbf{x}^*) \right) \tag{A7}$$

where

$$\mu_{y^*}(\mathbf{x}^*) = m(\mathbf{x}^*) + \mathbf{K}(\mathbf{x}^*, \mathbf{X}) \mathbf{K}(\mathbf{X}, \mathbf{X})^{-1} (\mathbf{y} - \mathbf{m}(\mathbf{X})) \tag{A8}$$

$$\sigma_{y^*}^2(\mathbf{x}^*) = k(\mathbf{x}^*, \mathbf{x}^*) - \mathbf{K}(\mathbf{x}^*, \mathbf{X}) \mathbf{K}(\mathbf{X}, \mathbf{X})^{-1} \mathbf{K}(\mathbf{x}^*, \mathbf{X})^T \tag{A9}$$

References

1. Bradley BA. A critical examination of seismic response uncertainty analysis in earthquake engineering. *Earthquake Engineering & Structural Dynamics* 2013; 42(11): 1717–1729. doi: 10.1002/eqe.2331
2. Kazantzi AK, Vamvatsikos D, Lignos DG. Seismic performance of a steel moment-resisting frame subject to strength and ductility uncertainty. *Engineering Structures* 2014; 78: 69–77. doi: 10.1016/j.engstruct.2014.06.044
3. AISC 360-16 . *Specification for structural steel buildings*. Chicago, Illinois: American Institute of Steel Construction . 2016.
4. ASCE 7-16 . *Minimum design loads and associated criteria for buildings and other structures*. Reston, Virginia: American Society of Civil Engineers . 2017.
5. Melchers RE, Beck AT. *Structural reliability analysis and prediction*. Hoboken, New Jersey: John Wiley & Sons. 3rd ed. 2018
6. Gulvanessian H, Calgaro JA, Holicky M. *Designers' guideto Eurocode: Basis of structural design*. London: ICE Publishing. 2nd ed. 2012.
7. Beyer HG, Sendhoff B. Robust optimization – A comprehensive survey. *Computer Methods in Applied Mechanics and Engineering* 2007; 196(33): 3190–3218. doi: 10.1016/j.cma.2007.03.003
8. Elishakoff I, Ohsaki M. *Optimization and anti-optimization of structures under uncertainty*. London: Imperial College Press . 2010
9. Ohsaki M, Yamakawa M, Fan W, Li Z. An order statistics approach to multiobjective structural optimization considering robustness and confidence of responses. *Mechanics Research Communications* 2019; 97: 33–38. doi: 10.1016/j.mechrescom.2019.04.003
10. Do B, Ohsaki M. Gaussian mixture model for robust design optimization of planar steel frames. *Structural and Multidisciplinary Optimization* 2021; 63(1): 137–160. doi: 10.1007/s00158-020-02676-3
11. Do B, Ohsaki M. A random search for discrete robust design optimization of linear-elastic steel frames under interval parametric uncertainty. *Computers & Structures* 2021; 249: 106506. doi: 10.1016/j.compstruc.2021.106506
12. Do B, Ohsaki M, Yamakawa M. Bayesian optimization for robust design of steel frames with joint and individual probabilistic constraints. *Engineering Structures* 2021; 245: 112859. doi: 10.1016/j.engstruct.2021.112859
13. Beck JL, Chan E, Irfanoglu A, Papadimitriou C. Multi-criteria optimal structural design under uncertainty. *Earthquake Engineering & Structural Dynamics* 1999; 28(7): 741–761. doi: 10.1002/(SICI)1096-9845(199907)28:7<741::AID-EQE840>3.0.CO;2-6
14. Frangopol DM, Maute K. Life-cycle reliability-based optimization of civil and aerospace structures. *Computers & Structures* 2003; 81(7): 397–410. doi: 10.1016/S0045-7949(03)00020-8
15. Valdebenito MA, Schuëller GI. A survey on approaches for reliability-based optimization. *Structural and Multidisciplinary Optimization* 2010; 42(5): 645–663. doi: 10.1007/s00158-010-0518-6
16. Do B, Ohsaki M, Yamakawa M. Sequential mixture of Gaussian processes and saddlepoint approximation for reliability-based design optimization of structures. *Structural and Multidisciplinary Optimization* 2021; 64(2): 625–648. doi: 10.1007/s00158-021-02855-w
17. Beck AT, Gomes WJS. A comparison of deterministic, reliability-based and risk-based structural optimization under uncertainty. *Probabilistic Engineering Mechanics* 2012; 28: 18–29. doi: 10.1016/j.probengmech.2011.08.007
18. Ohsaki M, Kinoshita T, Pan P. Multiobjective heuristic approaches to seismic design of steel frames with standard sections. *Earthquake Engineering & Structural Dynamics* 2007; 36(11): 1481–1495. doi: 10.1002/eqe.690
19. Foley CM, Pezeshk S, Alimoradi A. Probabilistic performance-based optimal design of steel moment-resisting frames. I: Formulation. *Journal of Structural Engineering* 2007; 133(6): 757–766. doi: 10.1061/(ASCE)0733-9445(2007)133:6(757)
20. Gong Y, Xue Y, Xu L, Grierson DE. Energy-based design optimization of steel building frameworks using nonlinear response history analysis. *Journal of Constructional Steel Research* 2012; 68(1): 43–50. doi: 10.1016/j.jcsr.2011.07.002
21. Papadrakakis M, Lagaros ND, Plevris V. Design optimization of steel structures considering uncertainties. *Engineering Structures* 2005; 27(9): 1408–1418. doi: 10.1016/j.engstruct.2005.04.002
22. Lagaros ND, Papadrakakis M. Robust seismic design optimization of steel structures. *Structural and Multidisciplinary Optimization* 2007; 33(6): 457–469. doi: 10.1007/s00158-006-0047-5
23. Liu Z, Atamturktur S, Juang CH. Reliability based multi-objective robust design optimization of steel moment resisting frame considering spatial variability of connection parameters. *Engineering Structures* 2014; 76: 393–403. doi:

10.1016/j.engstruct.2014.07.024
24. Geng X, Xie L. Data-driven decision making in power systems with probabilistic guarantees: Theory and applications of chance-constrained optimization. *Annual Reviews in Control* 2019; 47: 341–363. doi: 10.1016/j.arcontrol.2019.05.005
25. Zhao YG, Ono T. A general procedure for first/second-order reliabilitymethod (FORM/SORM). *Structural Safety* 1999; 21(2): 95–112. doi: 10.1016/S0167-4730(99)00008-9
26. Crestaux T, Le Maı^tre O, Martinez JM. Polynomial chaos expansion for sensitivity analysis. *Reliability Engineering & System Safety* 2009; 94(7): 1161–1172. doi: 10.1016/j.ress.2008.10.008
27. Caflisch RE. Monte Carlo and quasi-Monte Carlo methods. *Acta Numerica* 1998; 7: 1–49. doi: 10.1017/S0962492900002804
28. O'Hagan A. Bayes–Hermite quadrature. *Journal of Statistical Planning and Inference* 1991; 29(3): 245–260. doi: 10.1016/0378-3758(91)90002-V
29. Anderson TV, Mattson CA. Propagating skewness and kurtosis through engineering models for low-cost, meaningful, nondeterministic design. *Journal of Mechanical Design* 2012; 134(10): 100911. doi: 10.1115/1.4007389
30. Moustapha M, Sudret B. Surrogate-assisted reliability-based design optimization: a survey and a unified modular framework. *Structural and Multidisciplinary Optimization* 2019; 60(5): 2157–2176. doi: 10.1007/s00158-019-02290-y
31. Lignos DG, Krawinkler H. Deterioration modeling of steel components in support of collapse prediction of steel moment frames under earthquake loading. *Journal of Structural Engineering* 2011; 137(11): 1291–1302. doi: 10.1061/(ASCE)ST.1943-541X.0000376
32. Chopra AK. *Dynamics of structures: Theory and applications to earthquake engineering*. Hoboken, New Jersey: Prentice Hall. 4th ed. 2013.
33. Zareian F, Medina RA. A practical method for proper modeling of structural damping in inelastic plane structural systems. *Computers & Structures* 2010; 88(1): 45–53. doi: 10.1016/j.compstruc.2009.08.001
34. PEERC . PEER strong ground motion databases. "https://peer.berkeley.edu/peer-strong-ground-motion-databases"; 2021. [Accessed February 5, 2021].
35. Reyes JC, Kalkan E. How many records should be used in an ASCE/SEI-7 ground motion scaling procedure?. *Earthquake Spectra* 2012; 28(3): 1223–1242. doi: 10.1193/1.4000066
36. MathWorks . Statistics and machine learning toolbox user's guide (R2019b). "ttps://www.mathworks.com/help/stats"; 2019. [Accessed October 20, 2019].
37. Deb K, Pratap A, Agarwal S, Meyarivan T. A fast and elitist multiobjective genetic algorithm: NSGA-II. *IEEE transactions on evolutionary computation* 2002; 6(2): 182–197. doi: https://doi.org/10.1109/4235.996017
38. Zitzler E, Thiele L, Laumanns M, Fonseca CM, Fonseca dVG. Performance assessment of multiobjective optimizers: an analysis and review. *IEEE Transactions on Evolutionary Computation* 2003; 7(2): 117–132. doi: 10.1109/TEVC.2003.810758
39. Cao Y. Hypervolume indicator. "https://www.mathworks.com/matlabcentral/fileexchange/19651-hypervolume-indicator"; 2008. [Accessed October 10, 2020].
40. Lophaven SN, Nielsen HB, Søndergaard J. DACE-A Matlab Kriging toolbox, Version 2.0. Technical Report IMM-REP-2002-13, Technical University of Denmark; Lyngby, Denmark: 2002.
41. PEERC . Open System for Earthquake Engineering Simulation (OpenSees). "https://opensees.berkeley.edu/"; 2020. [Accessed December 10, 2020].
42. Regis RG, Shoemaker CA. A stochastic radial basis function method for the global optimization of expensive functions. *INFORMS Journal on Computing* 2007; 19(4): 497–509. doi: 10.1287/ijoc.1060.0182
43. Jones DR, Schonlau M, Welch WJ. Efficient global optimization of expensive black-box functions. *Journal of Global Optimization* 1998; 13(4): 455–492. doi: 10.1023/A:1008306431147
44. Rasmussen CE, Williams CKI. *Gaussian processes for machine learning*. Cambridge, Massachusetts: The MIT Press . 2006